



HAL
open science

Climatology of low-level clouds over western equatorial Africa based on ground observations and satellites.

Olivier Champagne, R. Aellig, A.H. Fink, Nathalie Philippon, Pierre Camberlin, V. Moron, P. Knippertz, G. Seze, R. van der Linden

► **To cite this version:**

Olivier Champagne, R. Aellig, A.H. Fink, Nathalie Philippon, Pierre Camberlin, et al.. Climatology of low-level clouds over western equatorial Africa based on ground observations and satellites.. *Journal of Climate*, 2023, 36 (13), pp.4289-4306. 10.1175/JCLI-D-22-0364.1 . hal-04168481

HAL Id: hal-04168481

<https://u-bourgogne.hal.science/hal-04168481>

Submitted on 9 Nov 2023

HAL is a multi-disciplinary open access archive for the deposit and dissemination of scientific research documents, whether they are published or not. The documents may come from teaching and research institutions in France or abroad, or from public or private research centers.

L'archive ouverte pluridisciplinaire **HAL**, est destinée au dépôt et à la diffusion de documents scientifiques de niveau recherche, publiés ou non, émanant des établissements d'enseignement et de recherche français ou étrangers, des laboratoires publics ou privés.

Journal of Climate

Climatology of low-level clouds over Western equatorial Africa based on ground observations and satellites --Manuscript Draft--

Manuscript Number:	JCLI-D-22-0364
Full Title:	Climatology of low-level clouds over Western equatorial Africa based on ground observations and satellites
Article Type:	Article
Corresponding Author:	Olivier Champagne Université Grenoble Alpes Saint Martin d'Hères, FRANCE
Corresponding Author's Institution:	Université Grenoble Alpes
First Author:	Olivier Champagne
Order of Authors:	Olivier Champagne Raffael Aellig Andreas H. Fink Nathalie Philippon Pierre Camberlin Vincent Moron Peter Knippertz Geneviève Seze Roderick Van Der Linden
Abstract:	<p>The tropical cloud forest ecosystem in Western Equatorial Africa (WEA) is known to be sensitive to the presence of an extensive and persistent low-level stratiform cloud deck during the long dry season from June to September (JJAS). Here we present a new climatology of the diurnal cycle of the low-level cloud cover from surface synoptic stations over WEA during JJAS 1971–2019. For the period JJAS 2008–2019, we also utilized estimates of cloudiness from three satellite products, namely the Satellite Application Facility on Support to Nowcasting and Very Short Range Forecasting (SAFNWC) cloud classification, the Day and Night Microphysical Schemes (DMS/NMS) and cross-sections from CALIPSO and CloudSat (2B-GEOPROF-LIDAR). A comparison with surface stations reveals that the NMS at night together with SAFNWC at daytime yield the smallest biases and highest Heidke skill scores. The climatological analysis reveals that low-level clouds persist during the day over the coastal plains and windward side of the low mountain ranges. Conversely, on their leeward sides, i.e. over the plateaus, a decrease of the low-level cloud frequency is observed in the afternoon, together with a change from stratocumulus to cumulus. At night, the low-level cloud deck reforms quickly over this region with the largest cloud occurrence frequencies in the morning. Vertical profiles from 2B-GEOPROF-LIDAR reveal cloud tops below 3000 m even at daytime. The station data and the suitable satellite products form the basis to better understand the physical processes controlling the clouds and to evaluate cloudiness from reanalyses and models.</p>

1 **Climatology of low-level clouds over Western equatorial Africa based on**
2 **ground observations and satellites**

3
4 O. Champagne^a, R. Aellig^b, A. H. Fink^b, N. Philippon^a, P. Camberlin^c, V. Moron^d, P.
5 Knippertz^b, G. Seze^e, and R. van der Linden^b

6 ^a *Institut des Géosciences de l'Environnement, Université Grenoble Alpes, CNRS, Grenoble, France*

7 ^b *Institute of Meteorology and Climate Research, Karlsruhe Institute of Technology, Karlsruhe, Germany*

8 ^c *Centre de Recherches de Climatologie, UMR 6282 Biogéosciences, CNRS/Université de Bourgogne Franche-*
9 *Comté, Dijon, France*

10 ^d *Aix Marseille Univ, CNRS, IRD, INRA, Coll France, CEREGE, F-13000 Aix-en-Provence, France*

11 ^e *LMD, IPSL, UPMC, CNRS, EP, ENS, 4 place Jussieu, F-75000 Paris, France*

12
13 *Corresponding author: Olivier Champagne, olivier.champagne@univ-grenoble-alpes.fr*
14

ABSTRACT

15

16 The tropical cloud forest ecosystem in Western Equatorial Africa (WEA) is known to be
17 sensitive to the presence of an extensive and persistent low-level stratiform cloud deck during
18 the long dry season from June to September (JJAS). Here we present a new climatology of
19 the diurnal cycle of the low-level cloud cover from surface synoptic stations over WEA
20 during JJAS 1971–2019. For the period JJAS 2008–2019, we also utilized estimates of
21 cloudiness from three satellite products, namely the Satellite Application Facility on Support
22 to Nowcasting and Very Short Range Forecasting (SAFNWC) cloud classification, the Day
23 and Night Microphysical Schemes (DMS/NMS) and cross-sections from CALIPSO and
24 CloudSat (2B-GEOPROF-LIDAR). A comparison with surface stations reveals that the NMS
25 at night together with SAFNWC at daytime yield the smallest biases and highest Heidke skill
26 scores. The climatological analysis reveals that low-level clouds persist during the day over
27 the coastal plains and windward side of the low mountain ranges. Conversely, on their
28 leeward sides, i.e. over the plateaus, a decrease of the low-level cloud frequency is observed
29 in the afternoon, together with a change from stratocumulus to cumulus. At night, the low-
30 level cloud deck reforms quickly over this region with the largest cloud occurrence
31 frequencies in the morning. Vertical profiles from 2B-GEOPROF-LIDAR reveal cloud tops
32 below 3000 m even at daytime. The station data and the suitable satellite products form the
33 basis to better understand the physical processes controlling the clouds and to evaluate
34 cloudiness from reanalyses and models.

35 1. Introduction

36 Many tropical wet forest ecosystems are tightly linked to the presence of low-level
37 clouds. These clouds reduce water demand and favor photosynthesis by enhancing diffuse
38 radiation (Karger et al. 2021), and in montane cloud forests they result in ‘hidden’
39 precipitation through leaf wetting (Berry and Goldsmith 2020; Goldsmith et al. 2013).
40 Western Equatorial Africa (WEA), encompasses southern Cameroon, Gabon and the
41 Republic of Congo and comprises the Ogooué and Kioulou-Niari basins as well as the Cristal
42 and Chaillu Mountains and Batéké plateau (Figure 1). It harbors large expanses of dense,
43 evergreen to semi-evergreen rain forests, whose presence is associated with a very high intra-
44 annual and inter-annual stability of the cloud cover (Wilson and Jetz 2016). Philippon et al.,
45 (2019 and 2022) have provided evidence of low solar irradiance and low sunshine duration
46 levels during the main dry season (June–September, JJAS) due to persistent low-level clouds.

47 Recent studies suggest a potential climate change threat on this forested region (Oliveira et al.
48 2014), and mainly a drying trend in Gabon (Bush et al. 2020) and an increase in shortwave
49 radiation further east in the Congo Basin (Burnett et al. 2020). Moreover, the years with very
50 warm sea surface temperatures in the eastern Atlantic favored less stratiform clouds in Gabon
51 (Maley and Hilaire 1993). Further back, a strengthening of the El Niño-Southern Oscillation
52 (ENSO) variability, likely forced the WEA rain forest to retreat 2000 years ago (Bayon et al.,
53 2019). This past retreat suggests a general vulnerability of this forest to climatic variations.
54 A potential threat through the ongoing climate change motivates the research on low-level
55 clouds in this region.

56 Despite these recent climatic trends and the potential high vulnerability of WEA forests
57 under climate change, very few studies have focused on the low-level clouds in WEA in
58 contrast to some neighboring regions such as the southeastern tropical and subtropical
59 Atlantic Ocean (Wood et al., 2012; Painemal et al., 2015), southern West Africa (SWA;
60 Kalthoff et al. 2018; Knippertz et al. 2011; Lohou et al. 2020; Schrage and Fink 2012;
61 Schuster et al. 2013; van der Linden et al. 2015) or the Namib desert in southwestern Africa
62 (Andersen and Cermak 2018; Andersen et al. 2019, 2020). The southeastern tropical and
63 subtropical Atlantic Ocean is covered by an extensive layer of marine stratus at the low-level
64 inversion (Wood 2012; Painemal et al. 2015). This is particularly so in boreal summer, when
65 the coastal upwelling extends northward to Cape Lopez (0°37'S) and the equatorial
66 upwelling cools the eastern equatorial Atlantic Ocean (Adebiyi and Zuidema 2018; Fuchs et
67 al. 2018; Hu et al. 2008). In SWA, low-level clouds are mainly present during the JJAS
68 monsoon season. At night the low-level clouds rapidly expand from the coast inland and peak
69 in the morning hours covering an area of nearly 800,000 km² (van der Linden et al. 2015).
70 The processes involved in the nighttime genesis and daytime lysis of the low-level clouds
71 involves a complicated multi-phase balance between cold air advection from the Atlantic
72 Ocean and divergence of net radiation and turbulent fluxes, partly in association with a
73 developing nighttime low-level jet (Knippertz et al. 2015; Lohou et al. 2020). On the
74 contrary, in the Namib region, low-level clouds form over the ocean during the night, are
75 advected to the land, and dissipate quickly in the morning (Andersen et al. 2020).

76 While the relative roles of cloud advection from the nearby Atlantic Ocean, orographic
77 cloud genesis, and boundary layer processes have not been assessed thoroughly for WEA yet,
78 a first important spatiotemporal climatology of low-level clouds was presented in Dommo et
79 al. (2018). They used station observations, satellite data, and the European Centre for

80 Medium-Range Weather Forecasts Interim reanalysis (Dee et al. 2011) over WEA to show
81 that dry season low-level cloud cover is developing in May, peaks in July-August and then
82 decreases again in October. These clouds tend to be more present in the morning, similarly to
83 what has been described for SWA (van der Linden et al. 2015). The low-level clouds are
84 more prevalent in the coastal plains and decrease inland, likely associated with a Foehn effect
85 leeward of the Chaillu, Cristal Mountains and Batéké Plateau (Fig. 1) leading to dissipation
86 of the cloud deck associated with the southwesterly to westerly low-level winds. The
87 formation of low-level clouds could also be favored by biomass burning aerosols that
88 increase air-mass stability (Solmon et al. 2021; Mallet et al. 2021).

89 Dommo et al. (2018) use the cloud classification from the Satellite Application Facility
90 on Support to Nowcasting and Very Short Range Forecasting (SAFNWC; (Derrien and Le
91 Gléau 2005), which has the advantage of a high spatial and temporal resolution and was
92 previously used to describe daytime low-level clouds in SWA (van der Linden et al., 2015).
93 However, SAFNWC has difficulties detecting very low-level clouds at night (van der Linden
94 et al., 2015) and a validation against in-situ synoptic observations was not performed
95 extensively in Dommo et al. (2018). Thus, the goal of the present study is to complement and
96 expand on the study by Dommo et al. (2018) In particular, our study relies on an improved
97 database for in-situ observations of clouds which contains more stations (62) over a longer
98 period (1971–2019). The spatial sampling is therefore increased, giving a better view of the
99 low-level clouds cover spatial pattern and conferring robustness to our results. The longer
100 overlap period between in-situ observations and satellite estimates (2008-2019 against 2008-
101 2009 in Dommo et al, 2018) enables computing scores of performances, thus quantitatively
102 evaluating the satellites datasets. In addition, we consider 8 genus of low clouds and not only
103 the total low clouds cover as in Dommo et al (2018). This allows us to precisely document (i)
104 the evolution from one genus to another along the diurnal cycle and (ii) how well these
105 different genera are detected by satellites. Lastly, we worked with (i) day and night
106 microphysical schemes (NMS/DMS, Lensky and Rosenfeld 2008) giving a more accurate
107 representation of the diurnal cycle of the low level cloud cover, and (ii) CALIPSO/CALIOP
108 data (namely the 2B-GEOPROF-LIDAR product, Mace and Zhang, 2014) to infer the cloud
109 cover vertical profile and cases when low clouds are under a multi-layered cover.

110 These points serve the overall goal of our study to present a description of the diurnal
111 cycle of the long dry season low-level cloud cover over Gabon and neighboring countries. It

112 should also provide a baseline to further investigate low-level clouds variability in the region
 113 as well as their realism in global and regional climate models simulations.

114 Section 2 will introduce the new set of in-situ observations and the satellite datasets,
 115 section 3 will present an extensive comparison between low-level clouds from SYNOP
 116 observations and from satellite data, and section 4 will discuss and summarize the main
 117 findings.



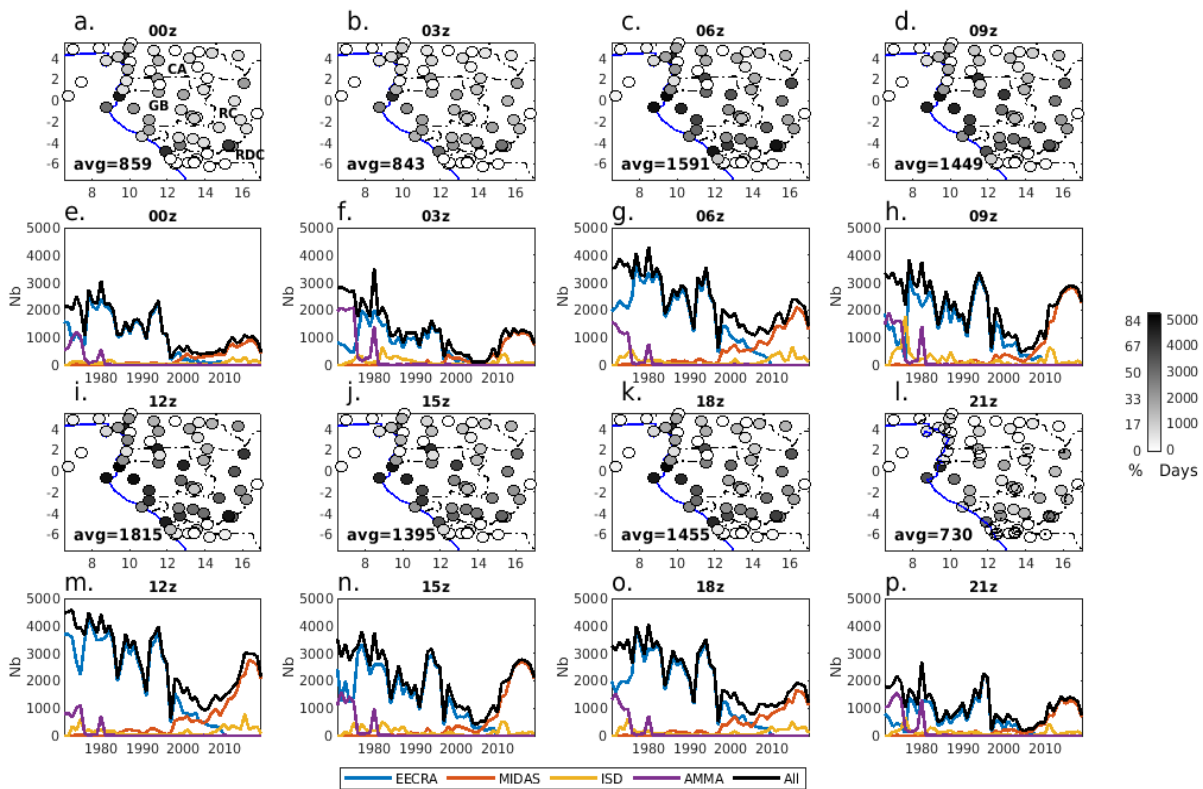
118
 119 Figure 1. Study region, names of main mountain ranges (terrain elevation from Danielson
 120 and Gesch, 2011) and location of stations used. The station marker size is proportional to the
 121 total number of available observations in the period 1971–2019. The altitudes are given in
 122 meters.

123 2. Data and Methods

124 *a. A comprehensive new dataset of cloud observations from stations*

125 The primary source of observed low-level cloud cover, including the low-level cloud
126 fraction (LCF) and the low-level cloud genus (LCG), is the “Extended Edited synoptic Cloud
127 Reports Archive” (EECRA, Hahn et al., 1999; Eastman and Warren, 2014) covering the
128 period until 2009. LCF is expressed in oktas and is of particular interest for a regional climate
129 perspective as it governs radiation reaching the surface. LCG uses the World Meteorological
130 Organization (WMO) coding into nine types (WMO 2019) plus two EECRA-specific types
131 (11 = obscure sky with fog; 10 = thunderstorm with showers). These two latter types were
132 omitted in this study (LCF coded to 0) because they result from ancillary information specific
133 to EECRA and not available in other datasets described below. The WMO low-level cloud
134 coding comprises cumulus (01 and 02), stratocumulus (04 and 05), stratus (06 and 07),
135 cumulus and stratocumulus (08), and cumulonimbus (03 and 09). In total, 62 stations were
136 extracted from EECRA for the period 1971–2009 and the region 5°N–6.5°S/6.5°–16.5°E
137 (Fig. 1). To fill in gaps and to update the EECRA database to 2019, three other databases
138 were used; these are in order of priority: The Met Office Integrated Data Archive System
139 (MIDAS, Met Office 2012), the Integrated surface database (ISD, Smith et al. 2011), and the
140 African Monsoon Multidisciplinary Analyses information system (AMMA, Fleury et al.
141 2011). MIDAS is less extensively used than EECRA but a data quality check (not shown) has
142 revealed better consistency than ISD and AMMA. ISD had some decoding problems from
143 2013, while our quality control lead us to conclude that AMMA should be given the lowest
144 priority. EECRA and the three additional sources are based on the same in-situ stations and
145 are therefore consistent in their common periods of records, as shown with the example of
146 Libreville (Fig. S1). From the latter three additional sources, three stations not in EECRA
147 were added: Franceville-Mvengue, Oyem (both in Gabon) and Mbanza Kongo (in Angola).
148 Inconsistent reports, where either LCG or LCF was zero and the respective other variable was
149 non-zero, were omitted. We also checked if the cloud observations could be enhanced by
150 hourly METAR (Meteorological aerodrome Reports) airport reports, but unfortunately the
151 cloud type coding is different and cloud fraction is not provided in oktas (Fig. S1).
152 Nevertheless, our merged in-situ cloud observations at synoptic stations (SYNOP
153 observations) are longer, more complete and more homogeneous than the in-situ observations
154 used in Dommo et al. (2018). The SYNOP observations have been published alongside this
155 article (Aellig et al. 2022).

156 SYNOP observations are carried out by trained observers eight times a day at main (00,
 157 06, 12, and 18 UTC) and intermediate (03, 09, 15, 21 UTC) synoptic hours. Note that the
 158 local time is UTC+1h. The location of stations, the total number of observations available,
 159 and their temporal evolution for each source and observation time can be inferred from Fig.
 160 2. Overall, the number of available observations decreased over time but increased again in
 161 the late 2000s. Stations in Gabon and Republic of Congo (RC) are the best documented,
 162 matching with the cloudiest region of WEA (Dommo et al. 2018; Philippon et al. 2019).
 163 Generally, more daytime (Fig. 2c,d,i,j) than nighttime (Fig. 2a,b,k,l) recordings were
 164 available (compare 00 UTC to 12 UTC) due to daytime-only operation at several stations.



165
 166 Figure 2. a-d and i-l: Number of JJAS observations available per stations at 3-hourly time
 167 steps(maps). The average number of observations for all stations is depicted in the bottom-left
 168 corner. e-h and m-p: Total number of JJAS observations (all stations) per year and data source
 169 at 3-hourly time steps (line graphs). Letters in the first panel indicate country names
 170 (CA=Cameroon, GB=Gabon, RC=Republic of the Congo, RDC= Democratic Republic of the
 171 Congo).

172 *b. Satellite products*

173 1) CLOUD TYPE FROM SAFNWC

174 The cloud type (CT) product from SAFNWC consists of a classification into 14 types
 175 available at 3 km spatial and 15-minute temporal resolutions over Europe and Africa from

176 2008 to 2019 (Derrien and Le Gléau, 2005). This product is based on the Spinning Enhanced
177 Visible and Infrared Imager (SEVIRI), a passive sensor with 12 different spectral channels
178 on-board the Meteosat Second Generation geostationary satellite (Schmetz et al., 2002). To
179 construct the SAFNWC CT product, cloud detection and cloud type classification are
180 performed using series of threshold tests applied sequentially: tests on reflectance and
181 window channel brightness temperature at 10.8 μm and differences in brightness temperature
182 between two wavelengths (chosen among 10.8, 12, 3.9, 8.7 μm). The used thresholds depend
183 on illumination, viewing geometry and geographical location, and are computed from a
184 radiative transfer model using ancillary data. Additional tests on spatial and temporal
185 variability of the brightness temperature at 10.8 μm and spatial variability of the reflectance
186 are also used. A detailed description of the SAFNWC CT algorithm can be found in Derrien
187 et al. (2013).

188 In our study, SAFNWC CTs are extracted for the WEA domain 5°N–6.5°S/6.5°–16.5°E
189 and the 2008–2019 period. For simplification and following Dommo et al 2018, the 14 CTs
190 were recombined into seven CTs: cloud free, very low clouds (up to 2000 meters above sea
191 level (a.s.l.)), low clouds (2000–3500 meters a.s.l.), mid-level clouds (3500–6500 meters
192 a.s.l.), high opaque clouds, high semi-transparent clouds (the latter two higher than 6500
193 meters a.s.l.), and finally fractional clouds (i.e. small cumulus, thin low or mid-level cloud
194 edges, very thin high cloud edges, broken and thin mid-level and low-level clouds). Cloud
195 type maps with the seven types are shown as examples in Figure 3b and 3e for 21 August
196 2015 12 UTC and 11 July 2010 00 UTC.

197 2) NIGHT- AND DAY-MICROPHYSICAL-SCHEMES

198 The Night-Microphysical-Scheme (NMS) and the Day-Microphysical-Scheme (DMS) are
199 based on radiances and reflectances in the visible and infrared (IR) channels of SEVIRI
200 (Lensky and Rosenfeld, 2008; Schmetz et al., 2002). The schemes are based on three
201 different channel combinations, which are combined to RGB composites. The DMS is a
202 combination of the solar reflectance in the visible channel at 0.8 μm (red) and at 3.9 μm
203 (green), and of the brightness temperature of the IR channel at 10.8 μm (blue). The 0.8 μm
204 channel is a measure of the cloud optical depth and amount of cloud water and ice. The 3.9
205 μm visible channel is a qualitative measure for cloud particle size and phase (Lensky and
206 Rosenfeld, 2008). The NMS uses the difference of the brightness temperatures of the IR
207 channels between 10.8 and 12.0 μm (red), and between 3.9 and 10.8 μm (green), and the
208 brightness temperature of the IR channel at 10.8 μm represented in blue (Lensky and

209 Rosenfeld, 2008). The channels represented with green are sensitive to particle size of
210 hydrometeors and the channels represented in red are a measure of the opaqueness of clouds.
211 Figures 3a and 3d show examples of DMS and NMS for 21 August 2015 12 UTC and 11 July
212 2010 00 UTC with the RGB NMS and DMS cloud classification by EUMeTrain (2017).
213 From these schemes, we distinguish for every grid point (3km x 3km) three categories: low
214 clouds, higher clouds and clear skies. The low-level cloud cover in DMS is determined by a
215 reflectance of more than 25% in the 0.8 μm visible channel and a brightness temperature
216 (10.8 μm) greater than 283 K, while during the night the low-level cloud cover in the NMS is
217 determined by a difference between the brightness temperature of the channels 12.0 and 10.8
218 μm greater than 2 K and a brightness temperature of channel 10.8 μm greater than 283 K. The
219 thresholds for NMS to detect low-level cloud cover have been used already in former studies
220 (van der Linden et al., 2015). 283 K represents the temperature at about 3000 m a.s.l. in the
221 study region, likely the upper limit of low-level clouds. In both DMS and NMS, brightness
222 temperatures lower than 283 K are considered as higher clouds.

223 3) CLOUDSAT/CALIPSO CPR/CALIOP (2B-GEOPROF-LIDAR)

224 The 2B-GEOPROF-LIDAR product is a merged product of data from the Cloud-Aerosol
225 Lidar with Orthogonal Polarization (CALIOP) lidar aboard CALIPSO (Winker et al., 2003)
226 and the Cloud Profiling Radar (CPR) aboard CloudSat (Stephens et al., 2002). Mace and
227 Zhang (2014), developed the 2B-GEOPROF-LIDAR product combining both profiles,
228 getting the most out of the information from both satellites. These two satellites are in the A-
229 train constellation circling around the earth in about 90 minutes and having a repeat period of
230 16 days until they sample the same swath again. They scan WEA on an ascending path from
231 the southeast to the northwest between 12:20 and 13:15 UTC, and on a descending path from
232 the northeast to the southwest between 23:20 UTC and 00:15 UTC. The time periods
233 available were JJAS 2006-2017 for daytime and JJAS 2006-2010 for nighttime. The CPR can
234 penetrate more optically thick clouds, while CALIOP can detect thin clouds and clouds close
235 to the surface (Mace et al., 2009; Marchand et al., 2008). An illustrative example for West
236 Africa is given in Knippertz et al. (2011). 2B-GEOPROF-LIDAR has a spatial resolution of
237 around 1.4 km along track, about 1.8 km cross track, and about 250 m vertically (Mace et al.,
238 2009). In WEA, the swaths have a zonal distance of around 170 km between each other.

239 4) SPATIAL REPRESENTATION OF THE THREE SATELLITE PRODUCTS

240 To qualitatively illustrate the performance of the different satellite products at day and
241 night, Fig. 3 provides examples for 1200 UTC 21 August 2015 and 0000 UTC 11 July 2010.
242 At daytime (top panels), both the SAFNWC and DMS represent the low-level clouds over
243 Gabon and the adjacent ocean similarly. In the 2B-GEOPROF-LIDAR product, the high
244 clouds over Cameroon and northern Gabon, likely stemming from deep convection, are
245 represented by high opaque and semi-transparent clouds in SAFNWC. At night (bottom
246 panels), the difficulty in the detection of low-level clouds by SAFNWC as opposed to NMS
247 is clearly visible over central and northern Gabon. 2B-GEOPROF-LIDAR shows the
248 thickened high-level clouds over the northern part of the region, which potentially prevents
249 detection of low-level clouds underneath. A close inspection of Fig. 3f reveals that 2B-
250 GEOPROF-LIDAR can detect low-level clouds underneath higher clouds, if the latter are
251 thin.

252 5) CLIMATOLOGY OF LOW-LEVEL CLOUD COVER FROM SATELLITES

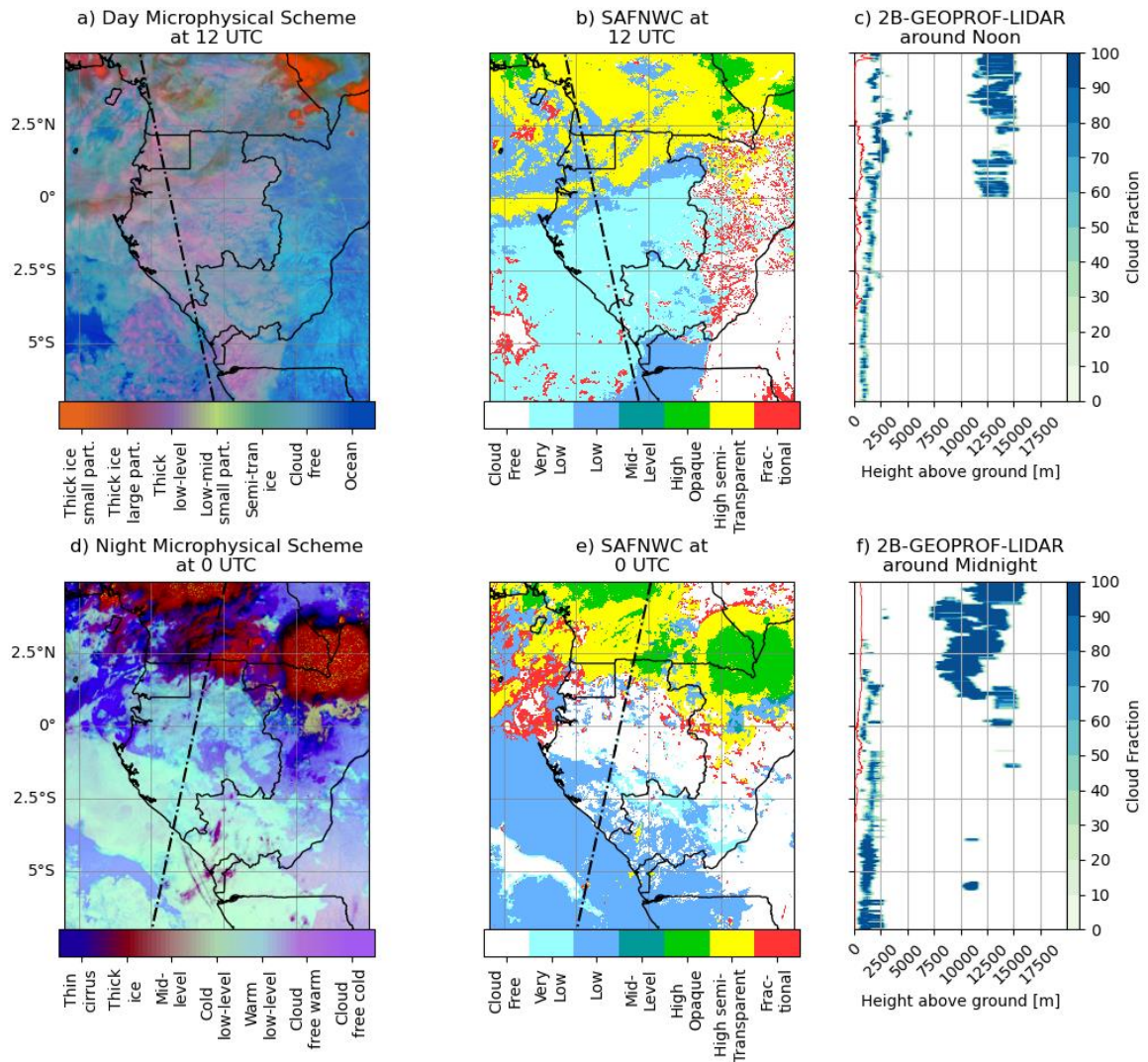
253 The climatology of low-level cloud cover was calculated for SAFNWC, DMS, NMS, and
254 2B-GEOPROF-LIDAR. These products do not provide LCF data, since only the presence or
255 absence of clouds in each pixel is detected. Hence, the climatology was primarily based on the
256 low-level cloud occurrence frequency (LCOF).

257 For SAFNWC, we calculated the average JJAS 3-hourly low-level cloud occurrence
258 frequency (LCOF) for the types of very low and low-level clouds at each grid point. Very low
259 clouds (top of the cloud under 2000 meters a.s.l) and low clouds (2000 — 3500 meters a.s.l.)
260 types are considered together for the calculation of LCOF because the top of the low-level
261 clouds detected in SYNOP (i.e. stratocumulus) can be situated above 2000 meters a.s.l. This
262 choice highlights the difficulty of comparing low level clouds from ground observations and
263 from satellites. At stations, clouds are seen from the ground and therefore determined according
264 to their base height (low, middle or high level) and type (9 possible categories). Cumulonimbus
265 clouds are for instance reported by WMO as low clouds (i.e. with a base height below 2000m
266 a.s.l.) despite their vertical extension. With satellites, clouds are determined according to their
267 top height, so cumuliform clouds are often classified as higher clouds and low clouds are
268 masked in case of a multilayered cloud cover. Therefore, the mismatch between ground
269 observations and satellite estimates of low level clouds can be quite large in the presence of
270 cumulus, cumulonimbus, or a multilayered cloud cover. The grid points characterized by

271 fractional clouds were also reassigned to another cloud type when at least half of the eight
272 surrounding points belonged to that type, following the method in Dommo et al. (2018). This
273 reassignment was made because the number of fractional clouds is not negligible and this type
274 appears spatially as a transition between two types (cf. Fig. 3). LCOF at each grid point and
275 observation time was obtained by calculating the ratio of the number of occurrence of very
276 low-level, low-level or reassigned fractional days to the total number of days, excluding higher
277 clouds (mid, high opaque and high semi-transparent). This method counters the problem of
278 low-level clouds not detected due to clouds situated above. The higher-level cloud occurrence
279 frequency was also calculated from the ratio of occurrence number of mid, high opaque, and
280 high semi-transparent cloud types to the total number of days.

281 For the climatology of low-level cloud cover based on NMS and DMS, we calculated for
282 each grid point the average JJAS 3-hourly LCOF with the thresholds defined in section 2.b.2.,
283 but only using the data with a threshold of the brightness temperature ($10.8 \mu\text{m}$) greater than
284 283 K. With this approach we alleviated the problem of clouds situated above the low-level
285 clouds, similarly to the approach used to calculate LCOF from SAFNWC.

286 For the climatology of low-level cloud cover based on 2B-GEOPROF-LIDAR, we
287 calculated first the cloud fraction and the cloud occurrence frequency at each vertical level
288 (250m resolution) and for each 0.5° parts (roughly 56 km) along track of the swaths (see
289 section 2.b.3.) using the random-overlap method (Geleyn and Hollingsworth, 1979; Räisänen
290 et al., 2004). For the lowest 3000 meters a.s.l., we calculated the climatology of LCF and
291 LCOF with the maximum-random-overlap method (Geleyn and Hollingsworth, 1979). If
292 there were multiple contiguous low-level clouds present, the random overlap method
293 (Räisänen et al., 2004) was applied. These overlap assumptions follow the method used in
294 van der Linden et al. (2015).



295

296 Figure 3. Satellite products on 1200 UTC 21 August 2015 (a-c), and 0000 UTC 11 July
 297 2010 (d-f) representing Cloud types from Day-Microphysical-Scheme (a), Night-
 298 Microphysical-Scheme (d), and SAFNWC (b and e); and cloud height and fraction from 2B-
 299 GEOPROF-LIDAR (c and f). The black dotted line in a-b and d-e depicts the path of the
 300 satellite, the data of which are shown in panels c and f. The red line in c. and f. represents the
 301 elevation.

302 *c. Methods for comparing in-situ observations and satellite products*

303 Low-level cloud fraction (LCF) and low-level cloud genus (LCG) at synoptic weather
 304 stations (SYNOP observations) are assessed by trained observers. Despite the subjective
 305 assessment and problems at night due to low illumination, various previous studies have
 306 shown their great value in obtaining cloud climatology and verification against satellite
 307 observations over Africa (van der Linden et al. 2015).

308 For the comparison with satellite products, the LCF climatology was calculated at synoptic
 309 weather station for time steps when the cloud genus (LCG) was either “stratocumulus” (genus

310 4-5), “stratus” (6–7), or “stratocumulus and cumulus” (8). For all other low-level cloud genus
311 (1, 2, 3, 9, i.e. cumulus and cumulonimbus clouds), the corresponding low-level cloud fraction
312 was set to 0 oktas because these clouds are not strictly low-level clouds and likely seen as
313 higher clouds from the satellites. Note that genus 1 (cumulus humilis), is rare, as its frequency
314 of occurrence is less than 2% at night and about 6% at daytime. Thus, using cloud genera 4–8
315 for stratiform low-level clouds at stations and comparing it with satellite low-level clouds
316 appears a tolerable inconsistency. The Low cloud occurrence frequency (LCOF) for SYNOP
317 observations was calculated by counting the occurrence of LCF higher than 4 oktas. For the
318 evaluation of satellite products against SYNOP observations, we converted cloud occurrence
319 around SYNOP stations to cloud fraction. We took the distance-weighted (cosine function from
320 0 to $\pi/2$) average cloud fraction in a radius of 20 km around the station at the time of the
321 observation, under the assumption that the observer on the ground can classify clouds and their
322 fractional cover in the sky up to this distance (WMO, 2019). Very low clouds, low clouds and
323 fractional reassigned clouds (see section 2.2.5) are considered together for the calculation of
324 low cloud fraction, similarly to the calculation of LCOF described in section 2.2.5. For the
325 comparison of low-level cloud fraction from SYNOP observations and satellite data, days with
326 more than 50% of higher clouds in the 20km radius around a station were excluded from the
327 analysis. This condition was applied because high- and mid-level clouds prevent the detection
328 of lower clouds from the satellites.

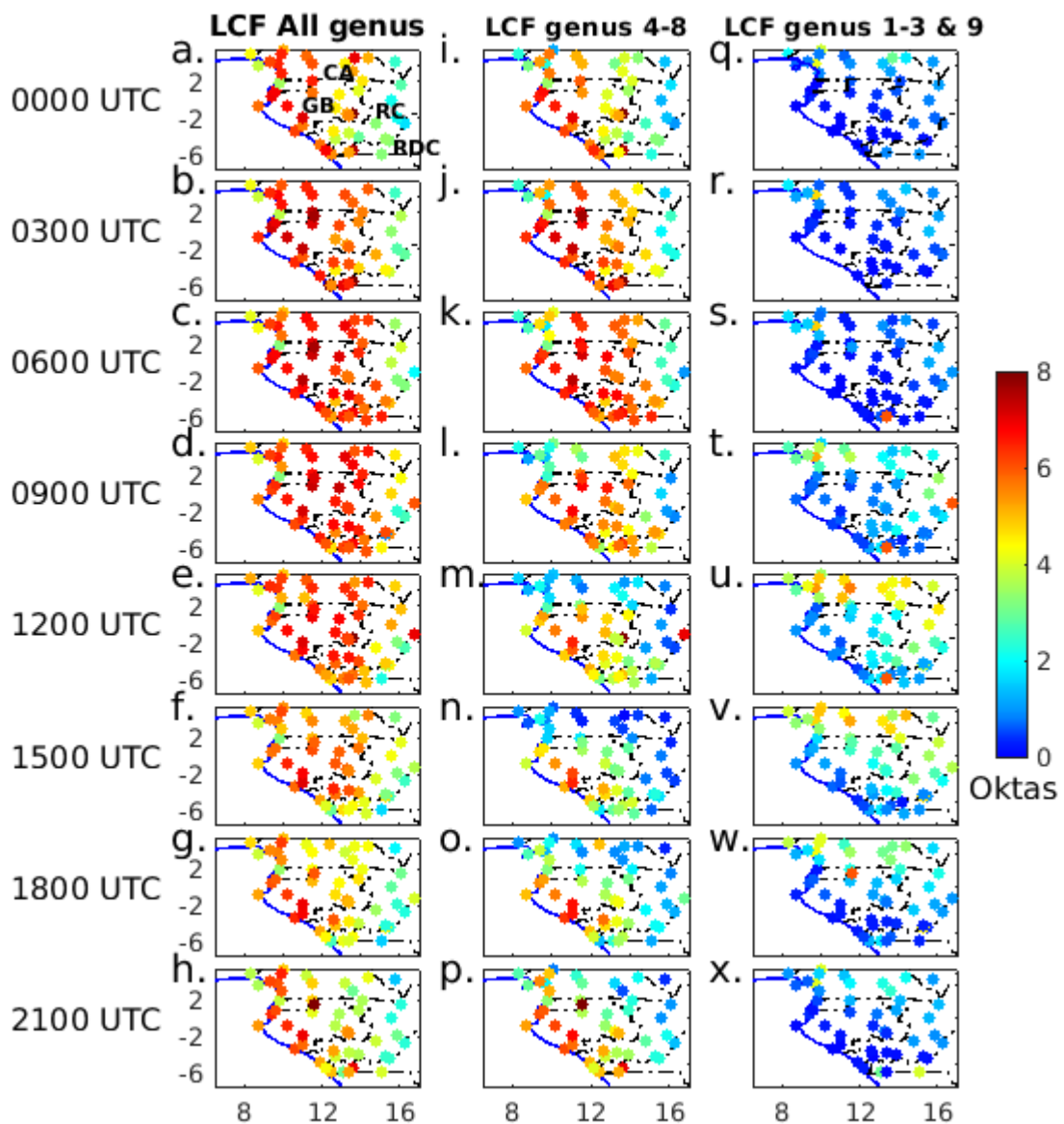
329 **3. Results**

330 This section shows in four parts the diurnal cycle of low-level clouds in WEA. The
331 first two parts explore the low-level cloud fraction and low-level cloud genus from SYNOP
332 observations on one hand and then the low-level cloud occurrence frequency from the three
333 satellite datasets on the other hand. The third part shows a comparison between SYNOP
334 observations and satellite data. The last part thoroughly compares the day and night evolution
335 of low-level clouds from SYNOP observations and satellite data.

336 *a. Ground observations of low-level cloud fraction and genus*

337 The long-term (JJAS 1971–2019) mean diurnal cycle of low-level clouds fraction (LCF) is
338 provided in Fig. 4. LCF with non-cumuliform clouds only (i.e. low topped low clouds, genus
339 4-8, Fig.4 i-p) and with only cumuliform clouds (genus 1-3 and 9, Fig. 4q-x) are also shown.
340 Taking LCF calculated from all genus, the cloud fraction is clearly lower toward the Congo

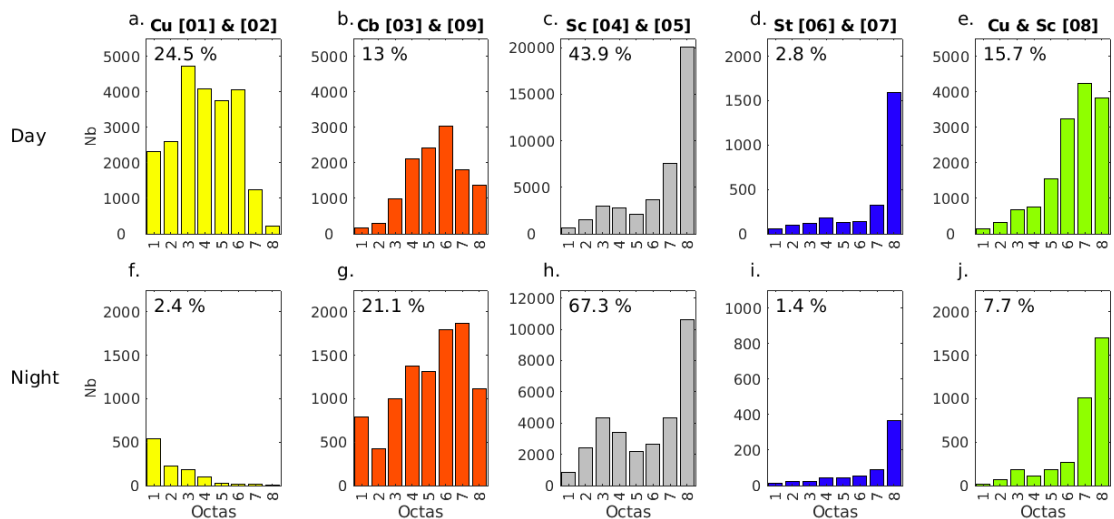
341 Basin in the east (Fig. 4a-h). In eastern Gabon, eastern Cameroon and southwestern RC, LCF
 342 increases at night (Fig. 4h,a,b), remains high until noon (Fig. 4e), and is followed by a decrease
 343 in the afternoon (Fig. 4f-g). When taking non cumuliform clouds only (Fig. 4l-n) the decrease
 344 is more pronounced and occurs earlier in eastern Gabon and Cameroon, showing that these
 345 regions are affected by convection and the development of cumuliform clouds in the daytime
 346 (Fig. 4t-v).



347
 348 Figure 4. JJAS (1971–2019) SYNOP low-level cloud fraction calculated from all genus (a-
 349 h), genus 4–8 only (i-p) and genus 1-3,9 only (q-x) per station and observation time.

350 The occurrence of cloud genus from SYNOP observations furnishes additional
 351 information regarding the type of low-level cloud cover in WEA (Fig. 5). Stratocumulus (Sc,

352 genus 04 and 05) is by far the most frequent type at night time (UTC 1800 – UTC 0300)
 353 representing two thirds of all cloud genus (Fig. 5f-j). The second most frequent cloud genus
 354 at night is cumulonimbus (Cb, genus 03 and 09) occurring at 21.1% of all observations.
 355 During daylight (UTC 0600 – UTC 1500, Fig. 5a-e), stratocumulus is less prominent but
 356 remains the most frequent (44%) followed by “cumulus humilis” and “mediocris” (Cu, genus
 357 01 and 02, 24.5%). The other main type is “cumulus and stratocumulus” (Cu & Sc, genus 08,
 358 15.7%). The occurrence of stratus (St, genus 06 and 07) is very low (1 to 3%) during day and
 359 night (Fig. 5d,i). It is likely that many clouds referred to as stratocumulus by observers are
 360 stratus. In any case stratus and stratocumulus are both counted as stratiform low level clouds.
 361 These results show that a significant number of low-level clouds are convective (Cu and Cb
 362 represent together 37.5% of all genus during the day and 23.5% at night). However, the
 363 portion of the sky covered by Cu and Cb is generally lower than Sc (oktas, x-axis of Fig. 5).
 364 Stratocumulus and stratus show a frequency distribution skewed to higher sky coverage (7-8
 365 oktas, Fig. 5c-d and Fig. 5h-i). For cumulus, the distribution shows a higher frequency
 366 between 3 and 6 oktas and a distribution even skewed to lower cloud coverage (Fig 5a). The
 367 distribution of Cumulonimbus is centered around 4-7 oktas but is skewed to higher cloud
 368 coverage during the day (Fig. 5b) while the distribution is flatter at night (Fig. 5g).

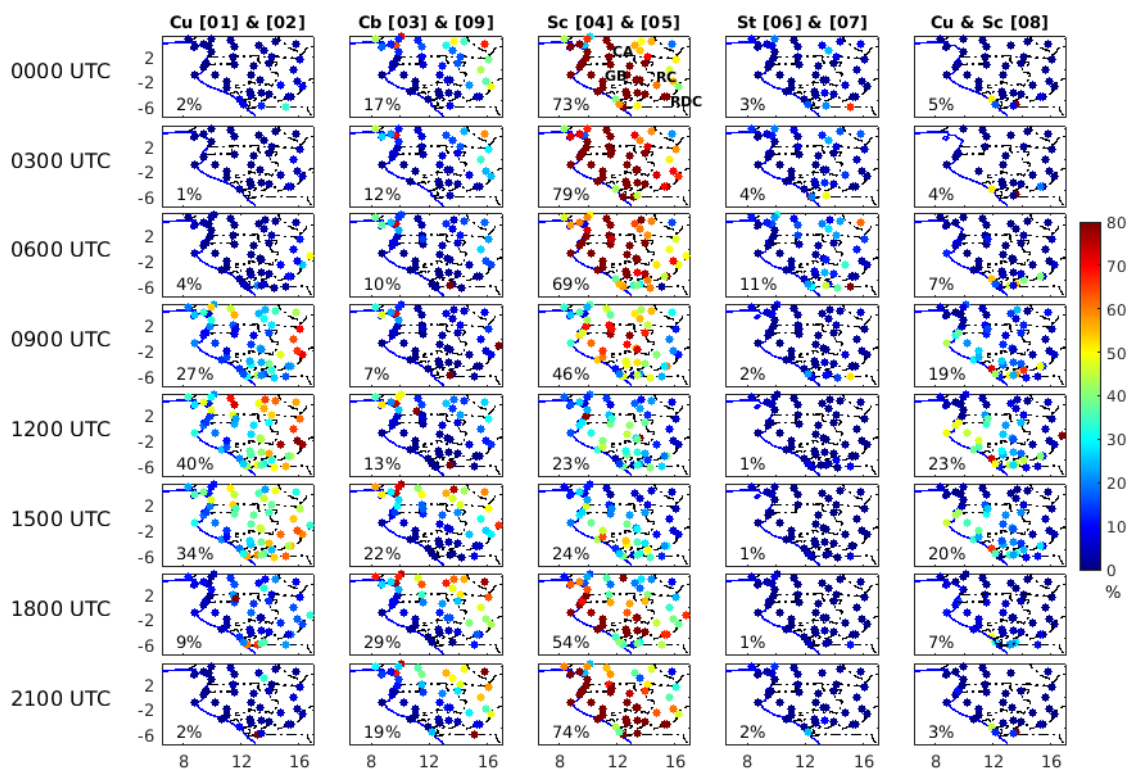


369

370 Figure 5. JJAS (1971-2019) number of SYNOP observations low-level cloud genus by
 371 oktas from all stations for daytime (06–15 UTC, a-e) and night-time (18–03 UTC, f-j).
 372 Percentages at the top give the frequency for each type over all SYNOP observation times.

373 The frequency of the cloud types varies spatially throughout the day (Fig. 6). At night (1800
 374 – 0300 UTC), the frequency of stratocumulus (genus 4 and 5) is high (>70%) especially in
 375 western Cameroon, Gabon and southwest RC. Some exceptions such as Porte-Gentil, show a

376 lower amount of Stratocumulus at night. The simultaneous higher amount of Sc and Cu (genus
 377 8), suggest that a specific cloud referencing by the observer in Port-Gentil might be the cause
 378 of this difference. In the morning, the amount of Sc markedly decreases everywhere but stays
 379 relatively high in the central part of Gabon. Simultaneously, the amount of cumulus (genus 1
 380 and 2) increases, especially in Cameroon and RC, where it reaches a maximum around 1200
 381 UTC. The cumulus & stratocumulus genus (genus 8) also reaches a maximum around 1200
 382 UTC, but occurs more frequently near the coast of Gabon. It reflects the breaking of the
 383 stratocumulus deck in the course of the day. Further, the stratus deck is more persistent on the
 384 windward slope of the Chaillu massif. The frequency of cumulonimbus (genus 3 and 9)
 385 increases later, reaching a maximum around 1800 UTC, located mostly in Cameroon and RC,
 386 while staying very low near the coast of Gabon and RC.



387

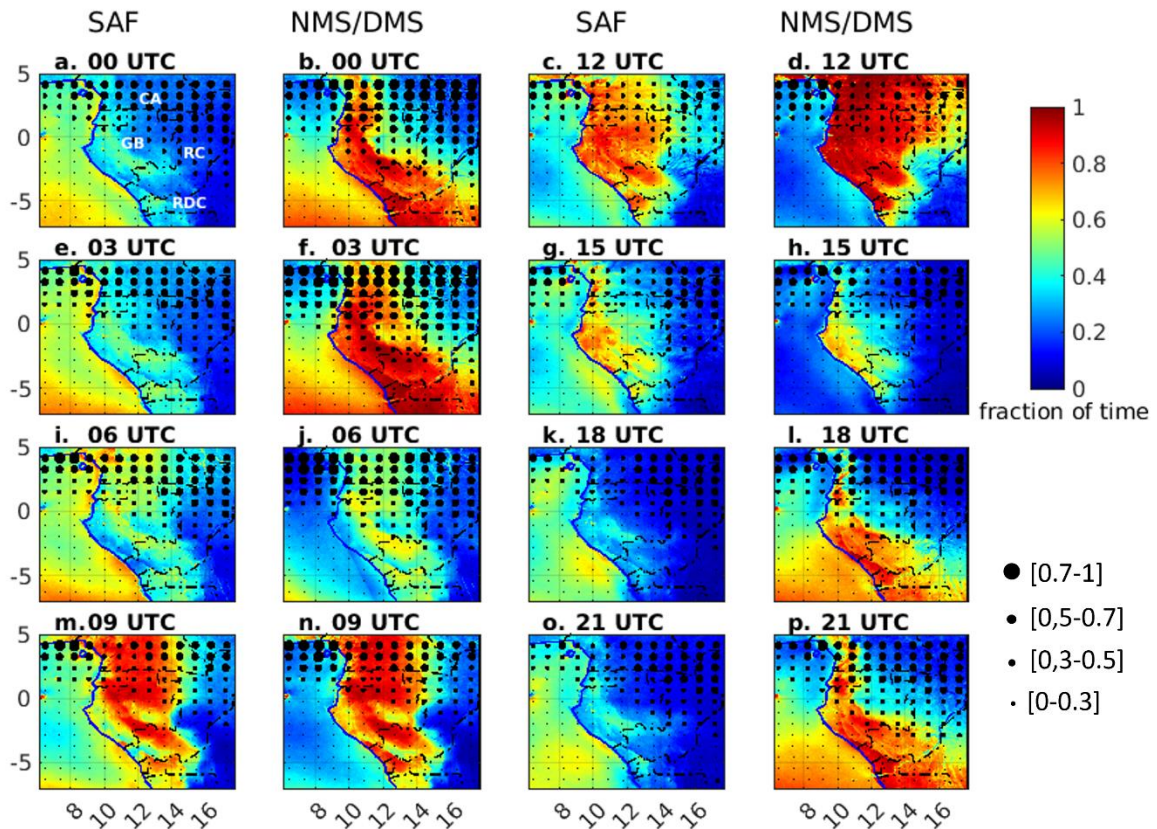
388 Figure 6. JJAS (1971–2019) SYNOP cloud genus occurrence frequency per station and
 389 observation time. For each panel, the number at the left bottom shows at each observation time
 390 the average fraction of the given cloud genus.

391 *b. Satellite observations of horizontal and vertical distributions of low-level clouds*

392 The average diurnal evolution of low-level cloud occurrence frequency (LCOF) from
 393 SAFNWC and NMS/DMS are displayed in Fig. 7 at the same 3-hourly time steps as in figure
 394 4. Between 0600 UTC and 0900 UTC, LCOF increases dramatically in both products (Fig.
 395 7i-j and 7m-n), likely associated with the low solar angle that prevents the satellite from

396 satisfactorily detecting low-level clouds just after the sunrise. This effect is conspicuous in
397 the first hour of daylight with a large LCOF increase observed between 0600 UTC and 0700
398 UTC (Fig. S2). In DMS, the increase of LCOF continues between 0900 UTC and 1200 UTC,
399 especially in Cameroon (Fig. 7n,d). Between 1200 UTC and 1500 UTC LCOF decreases in
400 the entire area, quite sharply with DMS (Fig. 7d,h), but stays high in western Gabon mainly
401 in SAFNWC (Fig. 7c,g). The lower LCOF in the eastern part of the region in the afternoon
402 suggests a sky clearing likely due to a transition from stratocumulus to cumulus shown in
403 SYNOP (Fig.6). Between 1500 UTC and 1800 UTC, corresponding to the period of the
404 switch from the DMS to the NMS, the evolution of LCOF is different between the two
405 satellite products SAFNWC (Fig. 7g,k) and the DMS/NMS microphysical scheme (Fig. 7h,l).
406 While the LCOF continues to decrease during sunset in SAFNWC (a constant decrease
407 according to Fig. S3), the LCOF starts to increase again in DMS/NMS, mainly in the coastal
408 area. After 1800 UTC and throughout the night LCOF increases again in both products, but
409 LCOF levels in NMS (Fig. 7b,f,l,p) are almost twice those of SAFNWC (Fig. 7a,e,k,o). The
410 increase of LCOF in NMS is again remarkable over the windward slopes and summit of the
411 main mountain ranges and the coast of RC and RDC and has a wider expansion along the
412 Chaillu Massif between 0000 UTC and 0300 UTC (Fig. 7b,f).

413 The higher-level cloud occurrence frequency (HCOF) from SAFNWC and NMS/DMS is
414 also shown in Fig.7 (black dots) and points out the areas of higher uncertainty in the detection
415 of low-level clouds from satellites. HCOF is larger in Cameroon, northern RC and northern
416 Gabon in both products and is increasing at night, reaching a 70% occurrence frequency in
417 Cameroon under NMS.

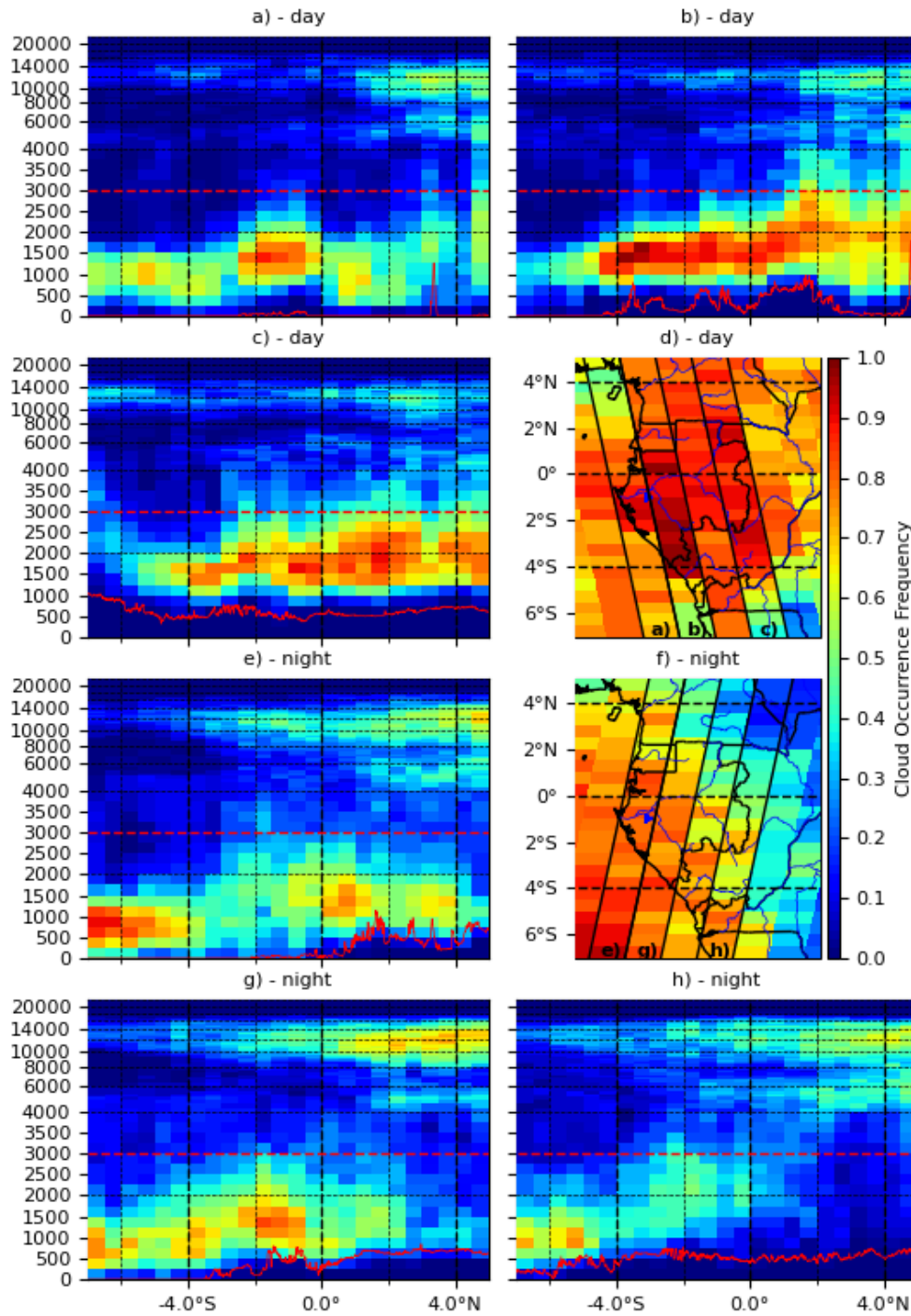


418
 419 Figure 7. JJAS Low-level clouds occurrence frequency (shading) and high clouds (dots)
 420 from SAFNWC and NMS/DMS for the eight observation times available at the analyzed
 421 stations in the period 2008–2019.

422 The twice-daily 2B-GEOPROF-LIDAR product does not allow to investigate the full
 423 diurnal cycle of the low-level cloud cover. However, it brings valuable information about
 424 clouds height, thickness and multilayers. Therefore, Figure 8 displays climatologies for
 425 around 12,30 UTC and 00,30 UTC of the vertical distribution (till 20km) of cloud occurrence
 426 frequency for six paths, and maps of LCOF (0-3000 meters a.s.l.). Around noon, the spatial
 427 variability of LCOF (Fig. 8d) is similar to the LCF (Fig. S4) and also similar to SAFNWC
 428 and DMS (Fig. 7c. and 7g.), namely a widespread stratiform deck in Gabon, the western part
 429 of RC and southwestern Cameroon. The main difference compared to SAFNWC is a larger
 430 number of low-level clouds near the coast of Gabon in 2B-GEOPROF-LIDAR (Fig. 8d). The
 431 vertical distribution of clouds also shows more low-level clouds from the coastal plains to the
 432 west of the Chaillu Massif (Fig. 8b, 4°S-2°N). The other main feature is a higher base of low-
 433 level clouds over land (Fig. 8b-c) compared to the ocean (Fig. 8a), which might be due to the
 434 elevated terrain (red line curves in Fig. 8a-c). The low-level clouds are also thicker north of
 435 2°S (up to 3000 meters). In addition, multilayered higher clouds become more frequent
 436 towards northern areas (Fig. 8a-c) and mask the low-level clouds when detected by passive
 437 sensors onboard satellites.

438 At mid-night the LCOF from 2B-GEOPROF-LIDAR (Fig. 8f) shows generally less low-
439 level clouds than at noon (Fig. 8d). A close inspection of Fig. 4i and 4m over central Gabon
440 corroborates this finding, only later in the night and in the early morning the LCOF increases
441 further and peaks in the diurnal cycle. In addition, the low-level clouds are more frequent near
442 the coast and their amount decreases inland towards the east (Fig. 8f), which is consistent with
443 the results found with SAFNWC (Fig. 7a,e,o) and NMS (Fig. 7b,f,p). The clouds might be
444 advected inland from the ocean, but because of the scarce twice-daily over-flights the dynamics
445 of the low-level clouds are difficult to estimate by 2B-GEOPROF-LIDAR. The vertical
446 distribution of clouds confirms the expanded stratus deck to the west, i.e. on the windward
447 slopes (Fig. 8e,g) while over the plateau further east (Fig. 1), the low-level cloud fraction is
448 lower (Fig. 8h). The role of the topography is shown here clearer compared to daytime (Fig.
449 8a-c), likely due to the SW-NE orientation of 2B-GEOPROF-LIDAR path followed at night
450 (Fig. 8f). In all night paths, there are also larger amounts of high level clouds over northern
451 Gabon, northern RC, and Cameroon (Fig. 8e,g-h), consistently with SAFNWC and NMS (Fig.
452 7a-b).

453 The results suggest a widespread stratiform cloud deck in the morning that clears up in
454 the afternoon mainly in the plateau east of Chaillu massif and Cristal mountains. However,
455 some inconsistencies between products have been found mainly due to the inability of
456 SAFNWC to detect low-level clouds at night. The multi-layered cloud cover mostly present
457 in northern Gabon and southern Cameroon at night as seen from 2B-GEOPROF-LIDAR,
458 may partly explain the lower number of low-level clouds detected with SAFNWC and
459 NMS/DMS there compared to SYNOP observations (Section 3.1). The aim of the next
460 section is to thoroughly compare SYNOP observations and satellite data.



461

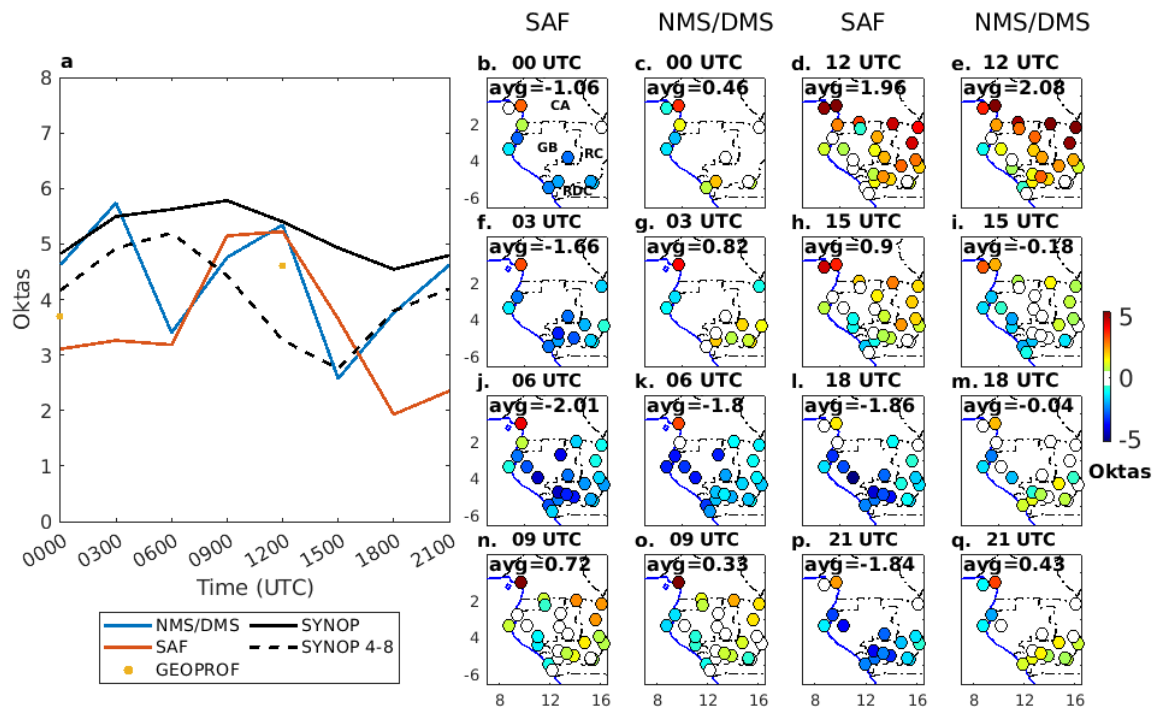
462 Figure 8. JJAS vertical cloud occurrence frequency from 2B-GEOPROF-LIDAR along
 463 three paths at 12:30 UTC (a,b,c) and three paths at 00:30 UTC (e,g,h) for the period 2006-2017
 464 during the day and 2006-2010 during the night. The red line is the topography. The LCOF
 465 calculated in each swath between the ground level and 3000 meters a.s.l. (horizontal red dotted
 466 line) are shown at 12:30 UTC (d.) and 00:30 UTC (f.)

467 *c. Comparison of satellite and station observations*

468 In this section, LCF from satellites and from SYNOP observations are compared. The
 469 average LCF in the entire area is very different between a LCF calculated with all SYNOP

470 genus or excluding cumuliform clouds (genus 4 to 8 only). During the day (1200 UTC-1500
471 UTC) the LCF excluding cumuliform clouds is lower by approximately 2 oktas. Focusing on
472 the latter, the highest level (more than 5 oktas) is reached at 0600 UTC (Fig. 9a). The LCF
473 decreases during the day to reach a minimum at 1500UTC (3 oktas). The diurnal cycle of LCF
474 from satellites is similar between SAFNWC and DMS during the day (0600 UTC – 1500 UTC,
475 Fig. 9a) with a peak at midday. In the early morning (0600 UTC) when the solar angle is low,
476 both satellite products underestimate the SYNOP observations because of a low illumination.
477 LCF from satellites overestimates SYNOP observations at midday (1200 UTC) when
478 cumuliform clouds are not counted in SYNOP observations (Fig. 9a). In the afternoon, satellite
479 products show a decrease of LCF, reaching a number close to SYNOP observations (around 3
480 oktas at 1500 UTC). At night (1800 UTC to 0300 UTC), LCF from SAFNWC shows a large
481 underestimation (2 oktas) compared to SYNOP observations while NMS show closer results
482 to SYNOP observations (Fig. 9a).

483 The bias between satellite datasets and SYNOP observations is highly dependent on the
484 region (Fig. 9b-q). At 0600 UTC the underestimation of LCF from satellites is larger in
485 western RC and western Gabon (Fig. 9j,k). During the day LCF starts to be overestimated
486 mainly in the north-east part of RC (Fig. 9n,o,d,e,h,i), where the cumuliform clouds are more
487 prevalent (Fig.6). At night (1800 UTC – 0300 UTC) less stations have a sufficient amount of
488 data for the analysis (mainly in central Gabon), which degrades the accuracy of the results,
489 but regional variability is still appearing. In western RC, a large underestimation appears in
490 SAFNWC (Fig. 9l,p,b,f) while NMS shows a slight overestimation (Fig. 9m,q,c,g). On
491 coastal Gabon, LCF is underestimated by a similar amplitude in both products. The bias in
492 termu of LCOF was also calculated (Figure S5) and show similar results. In addition, a
493 statistical analysis of the comparisons between SYNOP observations and satellite data is
494 shown in Fig. S6.



495

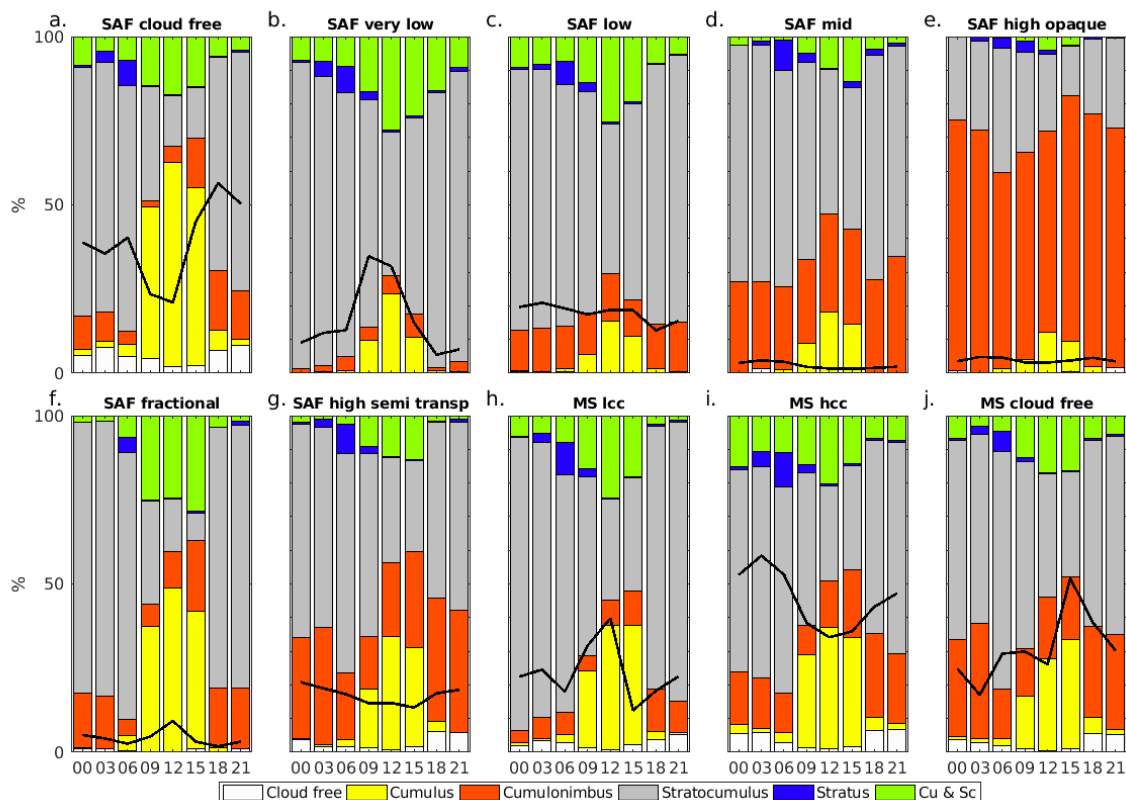
496 Figure 9. a. Spatially averaged diurnal cycle of LCF from SAFNWC, NMS (1800 UTC –
 497 0300 UTC), DMS (0600 UTC – 1500 UTC) and SYNOP observations (all genus and genus 4
 498 to 8 only). All stations have the same weight regardless of their sample size. b-q. Maps of the
 499 mean bias (in oktas) between LCF from SAFNWC or NMS/DMS and SYNOP observations
 500 (genus 4 to 8) for the period JJAS 2008–2019. “Avg” represents the average bias from all
 501 stations. The stations with less than 10% of available data have been removed from the analysis
 502 for each observation time.

503 The occurrence of low cloud genus from SYNOP observations and the occurrence of low
 504 cloud types from satellite data are finally compared to investigate how the satellites detect the
 505 different cloud genus. Figure 10 displays the diurnal cycle of the frequency of low-level
 506 cloud genus as observed at the stations (colored bars) for each satellite cloud type (individual
 507 panels).

508 Very low and low clouds together are the most frequent SAFNWC cloud types during the
 509 day (black line, Fig. 10) and are mostly detected when non-convective clouds
 510 (Stratocumulus) are observed from the ground (gray shade, Fig. 10b-c). Cloud free is detected
 511 more frequently at night and early morning (1800 UTC to 0600 UTC) and corresponds also
 512 mostly to stratocumulus (Fig. 10a), showing that a large part of stratiform clouds observed
 513 from the ground are not well detected by SAFNWC at night. As previously discussed in van
 514 der Linden et al. (2015), this is partly related to small temperature differences between low-
 515 level clouds and the ground, making it difficult to detect low-level clouds using IR brightness
 516 temperatures. In addition, high water vapor content in low levels makes it difficult to adjust

517 thresholds to detect cloudy pixels. During the day (0900 to 1500 UTC), Cumulus clouds
 518 prevail when no cloud is detected in satellites (Fig 10a.). Cumulus clouds are also frequent in
 519 the fractional type (Fig. 10f) due to the fractional characteristic of cumulus. Cumulus covers
 520 only a part of the sky (Fig. 5), so they are likely to be classified as cloud free in SAFNWC
 521 (Fig. 10a). The type “high semi-transparent” is also well represented and occurs steadily
 522 during the day at a frequency between 15 and 20% (black line, Fig. 10g). These high clouds
 523 from SAFNWC are associated with a significant number of stratocumulus in SYNOP
 524 observations (Fig. 10g) showing that the high clouds are likely hiding part of the
 525 stratocumulus situated underneath and seen from the ground.

526 The three DMS/NMS types include low-level clouds (MS lcc), higher level clouds (MS
 527 hcc) and cloud free (MS cloud free). These types have more inter-types similarities than
 528 SAFNWC in terms of partition of SYNOP cloud genus. The main difference among
 529 DMS/NMS types is a slightly higher proportion of stratocumulus in the low-level cloud type
 530 and a higher proportion of cumulonimbus in the cloud free type (Fig. 10h–j).



531

532 Figure 10. All stations diurnal partition of the SYNOP low-level cloud genus (colored
 533 bars) in the seven SAFNWC (“SAF” panels) and the three NMS/DMS (“MS” panels) cloud
 534 types for the period JJAS 2008–2019. The NMS was used from 18–03 UTC and the DMS
 535 from 06–15 UTC. Black line is the frequency of each SAFNWC cloud type relative to the

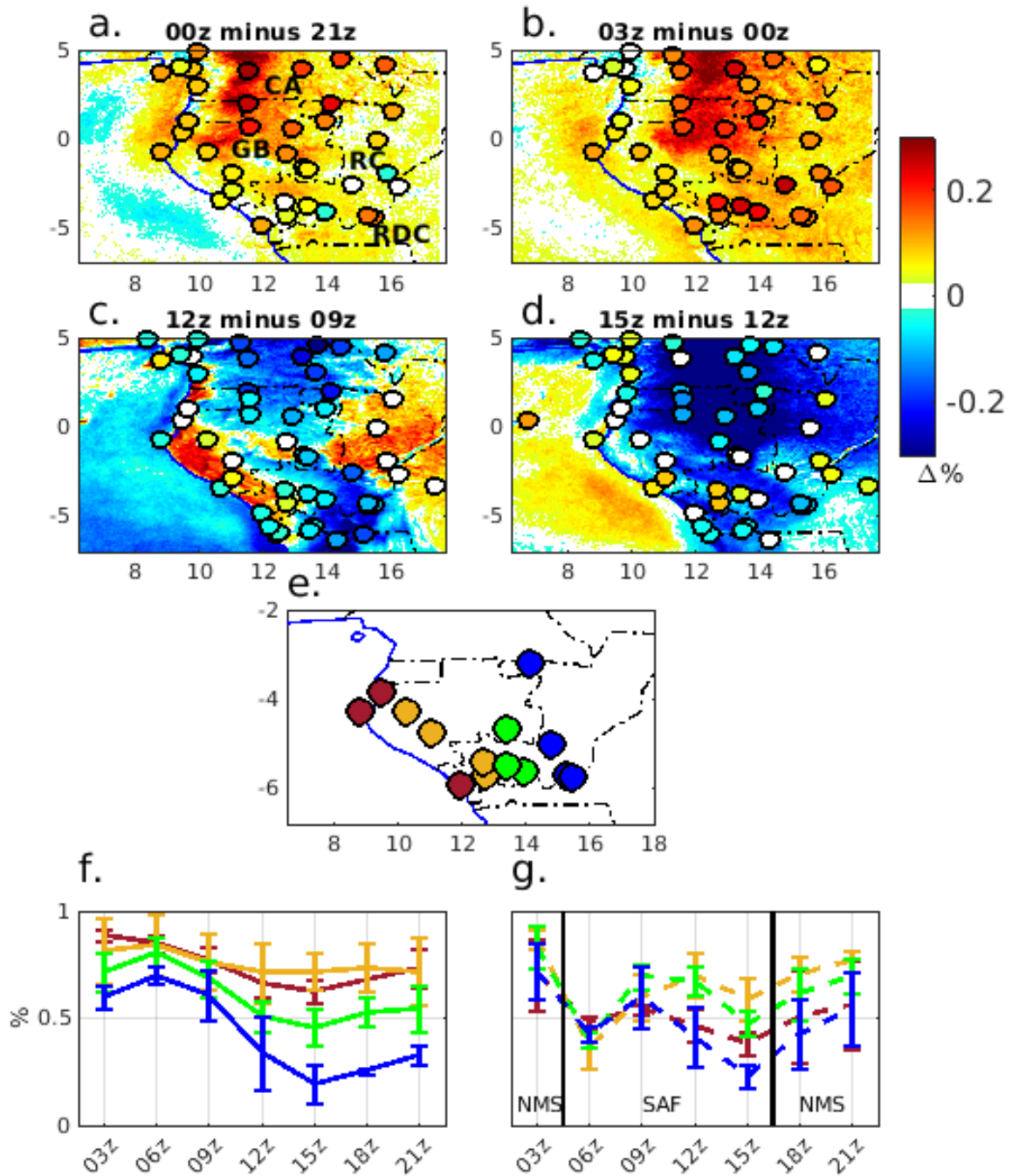
536 number of all available SYNOP observation days and stations. The stations with less than
537 10% of available data have been removed from the analysis for each observation time.
538

539 Overall, the comparison between SYNOP observations and satellite data described in this
540 section suggests clearly that NMS is more realistic than SAFNWC in detecting the low-level
541 clouds at nighttime. During the day, SAFNWC show similar LCF bias than DMS (Fig. 9) but
542 shows a higher proportion of stratocumulus detected as low clouds (Fig. 10).

543 *d. Spatial variability in the diurnal cycle of low-level cloud cover*

544 The previous section has shown large differences between SYNOP observations and
545 satellite products in absolute values of low-level cloud cover. Quantifying the change of low
546 cloud cover between successive observation times may therefore better reveal the spatial
547 consistencies of diurnal cycles in the different products. In this section, the evolution of JJAS
548 low-level cloud occurrence frequency (LCOF) between successive observation times in the
549 period 2008-2019 using NMS, SAFNWC and SYNOP observations is investigated (Fig. 11).
550 NMS is used for night time (Fig. 11a,b) and SAFNWC for day time (Fig. 11c,d) because these
551 products are more reliable in these respective periods, as shown in the previous section. 1800
552 UTC and 0600 UTC have been removed from this analysis since these times are not well
553 captured by the satellites (Fig. 9), due to twilight conditions.

554 The results from SYNOP observations show that low cloud occurrence frequency
555 increases in the evening, starting from western Gabon and western Cameroon, and spreading
556 to the east (Fig. 11a,b). The results from the NMS satellite data show a similar spatial
557 variability before midnight with the largest LCOF increase in the Cristal Mountains in
558 northern Gabon and in south-central Cameroon (Fig. 11a). After midnight and until 0300
559 UTC, the cloudiness keeps increasing in these regions, but also increases further east (Fig.
560 11b).



561

562 Figure 11: Change of low-level cloud occurrence frequency (LCOF) compared to the
 563 previous observation time for NMS (a-b) at nighttime and SAFNWC at daytime (c,d) for the
 564 period JJAS 2008-2019. The circles are the in-situ observed change LCOF in the period JJAS
 565 1971-2019 for stations with less than 10% of missing data. e) Location of the stations
 566 investigated in f) and g). f)-g): Average and standard deviation of LCOF from SYNOP
 567 observations (f) and satellites (g) at the coast (red), on the windward slopes and coastal plains
 568 (orange), on the plateau (green), and leeward slopes of Congo Basin (blue). The vertical lines
 569 in g) delineate the LCOF calculated from SAFNWC (06-15 UTC) and from NMS (18-03 UTC).

570

571 During the day, the SYNOP observations show generally a decrease of low-level cloud
 cover, but some stations show a very small change in LCOF, mainly in the central and northern

572 part of RC (Fig. 11c-d), most likely due to the development of low-level cumulus clouds (Fig.
573 6). A stable LCOF is also evident in the coastal hinterlands on the windward side of the Cristal
574 and Chaillu mountain ranges (Fig. 11c-d). The spatial variability of low cloud cover diurnal
575 evolution from SAFNWC is moderately consistent with the SYNOP observations: it shows an
576 increase in LCOF in the morning (0900 UTC - 1200 UTC) in the central and northern part of
577 RC and the coastal hinterlands, in regions of very low change of LCOF according to SYNOP
578 observations (Fig. 11c). Between 1200 UTC and 1500 UTC results from SAFNWC show a
579 general decrease of LCOF except for the coastal hinterlands, in line with a stable or slight
580 increase of LCOF in SYNOP observations (Fig. 11d).

581 To investigate the difference of mean diurnal cycle between different regions of the area,
582 stations with at least 10% of available data for each observation between 0300 and 2100 UTC
583 have been identified (Fig. 11e) and grouped according to their geographical locations. The
584 average SYNOP observations and SAFNWC LCOF diurnal cycle for these stations have been
585 calculated and reported on Fig. 11f and 11g. Looking at the SYNOP data, the coastal stations,
586 including Pointe-Noire, Mayumba, Port-Gentil and Libreville (in red) show very high LCOF
587 at night (80%), slightly decreasing during the day reaching 60% at 1500 UTC (Fig. 11f). The
588 windward slopes of the Chaillu mountains represented by the stations Dolisie, Makabana,
589 Tchibanga, Mouila and Lambarene (orange, cf. Fig. 1) are the cloudiest and show a steady
590 LCOF around 70-80%. Stations in the plateau region, including Mouyondzi, Sibiti, Franceville,
591 Lastoursville, Makokou and Mitzic (green) show a LCOF peaking at 80% around 0600 UTC
592 then decreasing in the afternoon to less than 50%. Further east in the region including
593 Brazzaville, Ndjili, Djambala and Souanké (blue, leeward slopes of plateau) the LCOF is
594 generally lower and shows a stronger diurnal cycle with LCOF varying between 70% in the
595 morning and 25% in the afternoon (Fig. 11f). Taking the grid point corresponding to each
596 station, SAFNWC during the day (0600 to 1500 UTC) and NMS at night (1800 to 0300 UTC)
597 the spatial variability of diurnal cycle is similar to SYNOP observations data (similar ranking
598 of the groups of stations; Fig. 11g). During the day, we observe an eastward gradient, with a
599 higher cloud occurrence frequency in the windward slopes and lower cloud cover toward the
600 inland region (Fig. 11g). At night (0000-0300 UTC) the difference of low-level cloud cover
601 between the windward slopes and the inland regions is reduced, similarly to SYNOP
602 observations (Fig. 11f-g). Inconsistencies between SYNOP observations and satellites include
603 a large underestimation of LCOF at 0600 UTC (see also Fig. 9) and a clear underestimation at
604 the coastal stations due to less low-level cloud over the ocean in SAFNWC.

605 The reduced low-level cloud cover over the plateau in the afternoon has been previously
606 associated to the topography favoring a foehn effect (Dommo et al. 2018). The afternoon
607 clearing occurring on the plateau may also be associated with a shortwave heating and a stronger
608 convection due to elevated terrain. The development of cumulus in eastern Gabon and central
609 RC supports this statement (Figure 6). The June-July daytime clearing of the low-level stratus
610 in southern Benin during the “convective phase”, as described in the conceptual model of
611 Lohou et al. (2020), provides a potential mechanism in this regard. However, a clear distinction
612 to the Benin site is the presence of a lush rainforest in Gabon and thus plant transpiration might
613 be of larger importance. After sunset, the LW cooling of the ground and later of the cloud top
614 might promote the formation of the clouds.

615 On the windward slopes of southern Cameroon, Equatorial Guinea, Gabon, and RC, the
616 apparent increase of low-level cloud cover during the morning in the satellites, while collocated
617 stations do not actually show any LCF increase (Figs. 7 and 11c), may be associated with an
618 elevation of the boundary layer that make the low-level clouds ‘visible’ to the satellite. Early
619 in the morning, the low-level cloud top temperature may not be significantly distinct from the
620 ground temperature, such that the low-level clouds can easily be misclassified as cloud-free by
621 the satellite’s algorithm. This result suggests a persistence of low-level level clouds as shown
622 in the SYNOP observations (Fig. 11f) more than a real increase in low-level cloud cover. To
623 the east of the coastal plains, at the western flank of the low mountain ranges, upslope winds
624 will support the persistence of clouds. While for West Africa, it was found that advection of
625 low-level marine stratus onto land plays an inferior role to the extent of the land-based stratus
626 (Lohou et al., 2020), this may be a contributor south of Port-Gentil where low-level offshore
627 clouds are frequent and widespread (Fig. 7).

628 Stations directly at the coast, like Port-Gentil at Cape Lopez and Pointe-Noire, but to a
629 lesser extent Libreville (red stations in Fig. 11e) exhibit a decrease of low-level cloud cover in
630 the morning, suggesting a frequent land-sea breeze activity, even during the cloudy dry season.
631 It is interesting to note that the coastal upwelling develops south of Port-Gentil (Herbert and
632 Bourlès 2018). Thus, the larger ocean-land temperature contrasts at Pointe-Noire and the “cape
633 location” of Port-Gentil may favor decrease of low-level cloud cover in the morning due to a
634 sea breeze.

635

636 4. Summary and Discussion

637 In this study, a data set of SYNOP observations of low cloud fraction and low cloud genus
638 of unprecedented length (1971–2019) and completeness has been compiled for Western
639 Equatorial Africa. It has been used to provide a climatology of low-level clouds and to evaluate
640 satellite cloud products, namely SAFNWC and NMS/DMS for the common period JJAS 2008-
641 2019. SAFNWC, NMS, and DMS products are based on the MSG SEVIRI multi-channel
642 radiometer and thus have a high spatial (3 km x 3 km) and temporal (15 minutes) resolution.
643 2B-GEOPROF-LIDAR which is based on the CloudSat CPR and Calipso CALIOP
644 instruments, and has a low sampling rate (two overflights per day and a return period of 16
645 days for the same swath), was also considered as it informs on the presence or not, of low-level
646 clouds in case of a multi-layered cloud cover.

647 Our evaluations of the satellite products (Figure 9) underscore the previously known
648 deficiencies of SAFNWC at detecting low-level clouds at night in tropical Africa (van der
649 Linden et al. 2015; Dommo et al. 2018) The lower skill of SAFNWC compared to NMS at
650 night is demonstrated by the proportion of undetected low-level clouds (all genera): in NMS
651 only ~25% (Fig. 10h) of the SYNOP low-level clouds are classified in the cloud free category
652 (among which a significant number of cumulonimbus), whereas in SAFNWC this number is
653 above 40% (Fig. 10b-c, and comprises mainly stratocumulus). Thresholds used in the NMS
654 algorithm are probably more efficient to capture low clouds, especially in case of a small
655 contrast between the ground and the cloud top temperature. A negative bias at night in
656 SAFNWC due to such a small contrast has previously been reported (van der Linden et al.
657 2015). Therefore, the use of the NMS, adapted for tropical conditions (Schrage and Fink, 2012)
658 is also recommended for WEA. Consequently, the concatenation of SAFNWC for daylight
659 hours (0600–1500 UTC) and NMS for nighttime (1800–0300 UTC) hours yields the most
660 realistic diurnal cycle compared to SYNOP observations, although caution should be exerted
661 around sunset and sunrise as both products show large biases. Our study clearly improves on
662 the results by Dommo et al. (2018) as this former study shows a maximum of low-level cloud
663 cover in the middle of the day in all parts of WEA, whereas low-level cloud cover (excluding
664 cumuliform clouds) peaks at late night /early morning.

665 The satellite products SAFNWC and NMS were together able to produce a similar spatial
666 variability of low-level clouds diurnal cycle compared to SYNOP observations. Mostly, over
667 the windward slopes of the Cristal and Chaillu mountains (Fig. 1), there is more low-level
668 clouds all day, while the plateau regions are characterized by a larger amplitude in the diurnal

669 cycle with higher LCOF in the morning, a decrease of LCOF (clearing) in the afternoon, and
670 low-level clouds that reform late at night (Figs. 7 and 11). However, frequent higher clouds,
671 making it impossible for most satellite instruments to detect clouds underneath, render the
672 results more uncertain in the northern part of the study region (i.e. South Cameroon, Fig. 7).
673 This higher cloud frequency is clear in the 2B-GEOPROF-LIDAR vertical profiles (Fig. 8). It
674 partly explains the larger underestimation of low-level clouds by SAFNWC and the
675 microphysical schemes compared to SYNOP observations in this region.

676 Despite uncertainties in both eye observations of clouds at stations and satellite cloud
677 products, the present study yields the most complete low-level cloud climatology for western
678 equatorial Africa to date and can provide a basis for further investigations on climate change
679 aspects of low-level clouds. First, this paper points to the observational and satellite products
680 that can be used for validating climate models over the historical period for the region. Second,
681 it documents the mean diurnal evolution of the low-level cloud cover and the spatial variability
682 of cloud fraction and frequency of occurrence. If models show a good performance at
683 reproducing these key characteristics over the historical period, then one should have some
684 confidence to use them for exploring the medium to long-term future evolution of the low-level
685 cloud cover. Coupled and forced CMIP6 models have still large deficiencies in simulating the
686 low-level oceanic and continental clouds in the region (Camberlin et al. 2022), but convection-
687 permitting model simulations, including sensitivity studies, should be suitable to shed more
688 light on the physical processes involved in the genesis and lysis of the low-level clouds..

689 *Acknowledgements.*

690 The authors thank the reviewers for their time spent on the manuscript and their valuable
691 comments. We also thank the AERIS/ICARE data center (<http://icare.univ-lille1.fr/>) for
692 providing access to the SAFNWC CT data used in this study. This study was part of the project
693 DYVALOCCA (<https://dyvalocca.osug.fr/>) funded by

694 ANR and DFG under Contract ANR-19-CE01-0021 and DFG FI 786/5-1

695 *Data availability statement.*

696 The datasets used to create the concatenated SYNOP dataset are from different sources :
697 EECRA is available at <https://rda.ucar.edu/datasets/ds292.2/#access>
698 ISD is from [https://www.ncei.noaa.gov/products/land-based-station/integrated-surface-](https://www.ncei.noaa.gov/products/land-based-station/integrated-surface-database)
699 [database.](https://www.ncei.noaa.gov/products/land-based-station/integrated-surface-database)

700 MIDAS is from <https://catalogue.ceda.ac.uk/uuid/220a65615218d5c9cc9e4785a3234bd0>.
701 SAFNWC is available upon request from the AERIS/ICARE data center (<http://icare.univ-lille1.fr/>).
702
703 DMS/NMS can be downloaded here
704 <https://data.eumetsat.int/product/EO:EUM:DAT:MSG:HRSEVIRI#>.
705 2B-GEOPROF-LIDAR is available here: [2B-GEOPROF-LIDAR | CloudSat DPC](https://www.colostate.edu/~geoprof/)
706 ([colostate.edu](https://www.colostate.edu))
707 The concatenated SYNOP observations dataset and the low cloud occurrence frequency and
708 low cloud fraction from SAFNWC, NMS/DMS and 2B-GEOPROF-LIDAR produced in this
709 study are available upon request.

710

711 REFERENCES

- 712 Adebisi, A. A., and P. Zuidema, 2018: Low Cloud Cover Sensitivity to Biomass-Burning
713 Aerosols and Meteorology over the Southeast Atlantic. *J. Clim.*, **31**, 4329–4346,
714 <https://doi.org/10.1175/JCLI-D-17-0406.1>.
- 715 Aellig, R., V. Moron, and P. Camberlin, 2022: Cloud observing data of 85 stations in western
716 Central Africa. <https://doi.org/10.5445/IR/1000150635>.
- 717 Andersen, H., and J. Cermak, 2018: First fully diurnal fog and low cloud satellite detection
718 reveals life cycle in the Namib. *Atmospheric Meas. Tech.*, **11**, 5461–5470,
719 <https://doi.org/10.5194/amt-11-5461-2018>.
- 720 ———, ———, I. Solodovnik, L. Lelli, and R. Vogt, 2019: Spatiotemporal dynamics of fog and
721 low clouds in the Namib unveiled with ground- and space-based observations.
722 *Atmospheric Chem. Phys.*, **19**, 4383–4392, <https://doi.org/10.5194/acp-19-4383-2019>.
- 723 ———, ———, J. Fuchs, P. Knippertz, M. Gaetani, J. Quinting, S. Sippel, and R. Vogt, 2020:
724 Synoptic-scale controls of fog and low-cloud variability in the Namib Desert.
725 *Atmospheric Chem. Phys.*, **20**, 3415–3438, <https://doi.org/10.5194/acp-20-3415-2020>.
- 726 Bayon, G., and Coauthors, 2019: The roles of climate and human land-use in the late
727 Holocene rainforest crisis of Central Africa. *Earth Planet. Sci. Lett.*, **505**, 30–41,
728 <https://doi.org/10.1016/j.epsl.2018.10.016>.
- 729 Berry, Z. C., and G. R. Goldsmith, 2020: Diffuse light and wetting differentially affect
730 tropical tree leaf photosynthesis. *New Phytol.*, **225**, 143–153,
731 <https://doi.org/10.1111/nph.16121>.
- 732 Burnett, M. W., G. R. Quetin, and A. G. Konings, 2020: Data-driven estimates of
733 evapotranspiration and its controls in the Congo Basin. *Hydrol. Earth Syst. Sci.*, **24**,
734 4189–4211, <https://doi.org/10.5194/hess-24-4189-2020>.
- 735 Bush, E. R., and Coauthors, 2020: Rare ground data confirm significant warming and drying
736 in western equatorial Africa. *PeerJ*, **8**, e8732, <https://doi.org/10.7717/peerj.8732>.

- 737 Camberlin, P., and Coauthors, 2022: The Representation of Dry-Season Low-Level Clouds
738 Over Western Equatorial Africa in Reanalyses and Historical CMIP6 Simulations.
739 *Submitted to Climate Dynamics*.
- 740 Danielson, J. J., and D. B. Gesch, 2011: *Global multi-resolution terrain elevation data 2010*
741 (*GMTED2010*). U.S. Geological Survey Open-File Report,.
- 742 Dee, D. P., and Coauthors, 2011: The ERA-Interim reanalysis: configuration and
743 performance of the data assimilation system. *Q. J. R. Meteorol. Soc.*, **137**, 553–597,
744 <https://doi.org/10.1002/qj.828>.
- 745 Derrien, M., and H. Le Gléau, 2005: MSG/SEVIRI cloud mask and type from SAFNWC. *Int.*
746 *J. Remote Sens.*, **26**, 4707–4732, <https://doi.org/10.1080/01431160500166128>.
- 747 ———, H. L. Gleau, and P. Fernandez, 2013: *Algorithm Theoretical Basis Document for*
748 *“Cloud Products” (CMa-PGE01 v3.2, CT-PGE02 v2.2 & CTTH-PGE03 v2.2)*.
749 [https://www.nwcsaf.org/AemetWebContents/ScientificDocumentation/Documentatio](https://www.nwcsaf.org/AemetWebContents/ScientificDocumentation/Documentation/MSG/SAF-NWC-CDOP2-MFL-SCI-ATBD-01_v3.2.1.pdf)
750 [n/MSG/SAF-NWC-CDOP2-MFL-SCI-ATBD-01_v3.2.1.pdf](https://www.nwcsaf.org/AemetWebContents/ScientificDocumentation/Documentation/MSG/SAF-NWC-CDOP2-MFL-SCI-ATBD-01_v3.2.1.pdf).
- 751 Dommo, A., N. Philippon, D. A. Vondou, G. Sèze, and R. Eastman, 2018: The June–
752 September Low Cloud Cover in Western Central Africa: Mean Spatial Distribution
753 and Diurnal Evolution, and Associated Atmospheric Dynamics. *J. Clim.*, **31**, 9585–
754 9603, <https://doi.org/10.1175/JCLI-D-17-0082.1>.
- 755 Eastman, R., and S. G. Warren, 2014: Diurnal Cycles of Cumulus, Cumulonimbus, Stratus,
756 Stratocumulus, and Fog from Surface Observations over Land and Ocean. *J. Clim.*,
757 **27**, 2386–2404, <https://doi.org/10.1175/JCLI-D-13-00352.1>.
- 758 EUMeTrain, 2017: Composite Image Quick Guide.
759 http://eumetrain.org/rgb_quick_guides/index.html (Accessed April 14, 2022).
- 760 Fleury, L., and Coauthors, 2011: AMMA information system: an efficient cross-disciplinary
761 tool and a legacy for forthcoming projects. *Atmospheric Sci. Lett.*, **12**, 149–154,
762 <https://doi.org/10.1002/asl.303>.
- 763 Fuchs, J., J. Cermak, and H. Andersen, 2018: Building a cloud in the southeast Atlantic:
764 understanding low-cloud controls based on satellite observations with machine
765 learning. *Atmospheric Chem. Phys.*, **18**, 16537–16552, [https://doi.org/10.5194/acp-18-](https://doi.org/10.5194/acp-18-16537-2018)
766 [16537-2018](https://doi.org/10.5194/acp-18-16537-2018).
- 767 Geleyn, J.-F., and A. Hollingsworth, 1979: An economical analytical method for the
768 computation of the interaction between scattering and line absorption of radiation.
769 *Beitr Phys Atmos*, **52**, 1–16.
- 770 Goldsmith, G. R., N. J. Matzke, and T. E. Dawson, 2013: The incidence and implications of
771 clouds for cloud forest plant water relations. *Ecol. Lett.*, **16**, 307–314,
772 <https://doi.org/10.1111/ele.12039>.
- 773 Hahn, C., S. Warren, and R. Eastman, 1999: Extended Edited Synoptic Cloud Reports from
774 Ships and Land Stations Over the Globe, 1952–2009 (NDP-026C).
775 <https://doi.org/10.3334/CDIAC/CLI.NDP026C>.
- 776 Herbert, G., and B. Bourlès, 2018: Impact of intraseasonal wind bursts on sea surface
777 temperature variability in the far eastern tropical Atlantic Ocean during boreal spring
778 2005 and 2006: focus on the mid-May 2005 event. *Ocean Sci.*, **14**, 849–869,
779 <https://doi.org/10.5194/os-14-849-2018>.
- 780 Hu, Z.-Z., B. Huang, and K. Pegion, 2008: Low cloud errors over the southeastern Atlantic in

- 781 the NCEP CFS and their association with lower-tropospheric stability and air-sea
782 interaction. *J. Geophys. Res.*, **113**, D12114, <https://doi.org/10.1029/2007JD009514>.
- 783 Kalthoff, N., and Coauthors, 2018: An overview of the diurnal cycle of the atmospheric
784 boundary layer during the West African monsoon season: results from the 2016
785 observational campaign. *Atmospheric Chem. Phys.*, **18**, 2913–2928,
786 <https://doi.org/10.5194/acp-18-2913-2018>.
- 787 Karger, D. N., M. Kessler, M. Lehnert, and W. Jetz, 2021: Limited protection and ongoing
788 loss of tropical cloud forest biodiversity and ecosystems worldwide. *Nat. Ecol. Evol.*,
789 **5**, 854–862, <https://doi.org/10.1038/s41559-021-01450-y>.
- 790 Knippertz, P., A. H. Fink, R. Schuster, J. Trentmann, J. M. Schrage, and C. Yorke, 2011:
791 Ultra-low clouds over the southern West African monsoon region: ULTRA-LOW
792 CLOUDS OVER WEST AFRICA. *Geophys. Res. Lett.*, **38**, n/a-n/a,
793 <https://doi.org/10.1029/2011GL049278>.
- 794 ———, and Coauthors, 2015: The DACCIWA Project: Dynamics–Aerosol–Chemistry–Cloud
795 Interactions in West Africa. *Bull. Am. Meteorol. Soc.*, **96**, 1451–1460,
796 <https://doi.org/10.1175/BAMS-D-14-00108.1>.
- 797 Lensky, I. M., and D. Rosenfeld, 2008: Clouds-Aerosols-Precipitation Satellite Analysis Tool
798 (CAPSAT). *Atmospheric Chem. Phys.*, **8**, 6739–6753, <https://doi.org/10.5194/acp-8-6739-2008>.
- 800 van der Linden, R., A. H. Fink, and R. Redl, 2015: Satellite-based climatology of low-level
801 continental clouds in southern West Africa during the summer monsoon season: Low-
802 level clouds in southern West Africa. *J. Geophys. Res. Atmospheres*, **120**, 1186–1201,
803 <https://doi.org/10.1002/2014JD022614>.
- 804 Lohou, F., N. Kalthoff, B. Adler, K. Babić, C. Dione, M. Lothon, X. Pedruzo-Bagazgoitia,
805 and M. Zouzoua, 2020: Conceptual model of diurnal cycle of low-level stratiform
806 clouds over southern West Africa. *Atmospheric Chem. Phys.*, **20**, 2263–2275,
807 <https://doi.org/10.5194/acp-20-2263-2020>.
- 808 Mace, G. G., and Q. Zhang, 2014: The CloudSat radar-lidar geometrical profile product (RL-
809 GeoProf): Updates, improvements, and selected results: CLOUDSAT RADAR-
810 LIDAR GEOMETRICAL PROFILE. *J. Geophys. Res. Atmospheres*, **119**, 9441–9462,
811 <https://doi.org/10.1002/2013JD021374>.
- 812 ———, ———, M. Vaughan, R. Marchand, G. Stephens, C. Trepte, and D. Winker, 2009: A
813 description of hydrometeor layer occurrence statistics derived from the first year of
814 merged Cloudsat and CALIPSO data. *J. Geophys. Res.*, **114**, D00A26,
815 <https://doi.org/10.1029/2007JD009755>.
- 816 Maley, J., and E. Hilaire, 1993: The role of clouds in the evolution of tropical African
817 palaeoenvironments. *Veille climatique satellitaire*. **46**, 51–63.
- 818 Mallet, M., P. Nabat, B. Johnson, M. Michou, J. M. Haywood, C. Chen, and O. Dubovik,
819 2021: Climate models generally underrepresent the warming by Central Africa
820 biomass-burning aerosols over the Southeast Atlantic. *Sci. Adv.*, **7**, eabg9998,
821 <https://doi.org/10.1126/sciadv.abg9998>.
- 822 Marchand, R., G. G. Mace, T. Ackerman, and G. Stephens, 2008: Hydrometeor Detection
823 Using Cloudsat—An Earth-Orbiting 94-GHz Cloud Radar. *J. Atmospheric Ocean.
824 Technol.*, **25**, 519–533, <https://doi.org/10.1175/2007JTECHA1006.1>.

- 825 Met Office, 2012: Met Office Integrated Data Archive System (MIDAS) Land and Marine
826 Surface Stations Data (1853-current).
827 <https://catalogue.ceda.ac.uk/uuid/220a65615218d5c9cc9e4785a3234bd0>.
- 828 Oliveira, R. S., C. B. Eller, P. R. L. Bittencourt, and M. Mulligan, 2014: The hydroclimatic
829 and ecophysiological basis of cloud forest distributions under current and projected
830 climates. *Ann. Bot.*, **113**, 909–920, <https://doi.org/10.1093/aob/mcu060>.
- 831 Painemal, D., K.-M. Xu, A. Cheng, P. Minnis, and R. Palikonda, 2015: Mean Structure and
832 Diurnal Cycle of Southeast Atlantic Boundary Layer Clouds: Insights from Satellite
833 Observations and Multiscale Modeling Framework Simulations. *J. Clim.*, **28**, 324–
834 341, <https://doi.org/10.1175/JCLI-D-14-00368.1>.
- 835 Philippon, N., and Coauthors, 2019: The light-deficient climates of western Central African
836 evergreen forests. *Environ. Res. Lett.*, **14**, 034007, <https://doi.org/10.1088/1748-9326/aaf5d8>.
- 838 Philippon, N., A. Ouhechou, P. Camberlin, J. Trentmann, A. H. Fink, J. D. Maloba, B. Morel,
839 and G. Samba, 2022: Characterization of Sunshine Duration in Western Equatorial
840 Africa: In Situ Measurements versus SARA-2 Satellite Estimates. *J. Appl. Meteorol.*
841 *Climatol.*, **61**, 185–201.
- 842 Räisänen, P., H. W. Barker, M. F. Khairoutdinov, J. Li, and D. A. Randall, 2004: Stochastic
843 generation of subgrid-scale cloudy columns for large-scale models. *Q. J. R. Meteorol.*
844 *Soc.*, **130**, 2047–2067, <https://doi.org/10.1256/qj.03.99>.
- 845 Schmetz, J., P. Pili, S. Tjemkes, D. Just, J. Kerkmann, S. Rota, and A. Ratier, 2002: An
846 Introduction to Meteosat Second Generation (MSG). *Bull. Am. Meteorol. Soc.*, **83**,
847 992–992, <https://doi.org/10.1175/BAMS-83-7-Schmetz-2>.
- 848 Schrage, J. M., and A. H. Fink, 2012: Nocturnal Continental Low-Level Stratus over Tropical
849 West Africa: Observations and Possible Mechanisms Controlling Its Onset. *Mon.*
850 *Weather Rev.*, **140**, 1794–1809, <https://doi.org/10.1175/MWR-D-11-00172.1>.
- 851 Schuster, R., A. H. Fink, and P. Knippertz, 2013: Formation and Maintenance of Nocturnal
852 Low-Level Stratus over the Southern West African Monsoon Region during AMMA
853 2006. *J. Atmospheric Sci.*, **70**, 2337–2355, <https://doi.org/10.1175/JAS-D-12-0241.1>.
- 854 Smith, A., N. Lott, and R. Vose, 2011: The Integrated Surface Database: Recent
855 Developments and Partnerships. *Bull. Am. Meteorol. Soc.*, **92**, 704–708,
856 <https://doi.org/10.1175/2011BAMS3015.1>.
- 857 Solmon, F., N. Elguindi, M. Mallet, C. Flamant, and P. Formenti, 2021: West African
858 monsoon precipitation impacted by the South Eastern Atlantic biomass burning
859 aerosol outflow. *Npj Clim. Atmospheric Sci.*, **4**, 54, <https://doi.org/10.1038/s41612-021-00210-w>.
- 861 Stephens, G. L., and Coauthors, 2002: THE CLOUDSAT MISSION AND THE A-TRAIN:
862 A New Dimension of Space-Based Observations of Clouds and Precipitation. *Bull.*
863 *Am. Meteorol. Soc.*, **83**, 1771–1790, <https://doi.org/10.1175/BAMS-83-12-1771>.
- 864 Wilson, A. M., and W. Jetz, 2016: Remotely Sensed High-Resolution Global Cloud
865 Dynamics for Predicting Ecosystem and Biodiversity Distributions. *PLOS Biol.*, **14**,
866 e1002415, <https://doi.org/10.1371/journal.pbio.1002415>.
- 867 Winker, D. M., J. R. Pelon, and M. P. McCormick, 2003: The CALIPSO mission: spaceborne
868 lidar for observation of aerosols and clouds. U.N. Singh, T. Itabe, and Z. Liu, Eds.,

- 869 Third International Asia-Pacific Environmental Remote Sensing Remote Sensing of
870 the Atmosphere, Ocean, Environment, and Space, Hangzhou, China, 1.
- 871 WMO, 2019: Identifying the genus | International Cloud Atlas.
872 <https://cloudatlas.wmo.int/en/identifying-the-genus.html> (Accessed October 21,
873 2021).
- 874 Wood, R., 2012: Stratocumulus Clouds. *Mon. Weather Rev.*, **140**, 2373–2423,
875 <https://doi.org/10.1175/MWR-D-11-00121.1>.